AD_____

Award Number: DAMD17-99-1-9144

TITLE: Optimization of Technique Factors for Full-Field Digital Mammography and Comparison of Optimized Techniques to Screen-Film Mammography

PRINCIPAL INVESTIGATOR: Eric A. Berns, Ph.D.
Dr. Edward Hendrick

CONTRACTING ORGANIZATION: Northwestern University
Evanston, IL 60208-1110

REPORT DATE: September 2003

TYPE OF REPORT: Annual Summary

PREPARED FOR: U.S. Army Medical Research and Materiel Command
Fort Detrick, Maryland 21702-5012

REPORT DOCUMENTATION PAGE

Form Approved
OMB No. 074-0188

1. AGENCY USE ONLY (Leave blank)	2. REPORT DATE	3. REPORT TYPE AND DATES COVERED
	September 2003	Annual Summary (1 Jul 1999 - 19 Aug 2003)

4. TITLE AND SUBTITLE
Optimization of Technique Factors for Full-Field Digital Mammography and Comparison of Optimized Techniques to Screen-Film Mammography

5. FUNDING NUMBERS
DAMD17-99-1-9144

6. AUTHOR(S)
Eric A. Berns, Ph.D.
Dr. Edward Hendrick

7. PERFORMING ORGANIZATION NAME(S) AND ADDRESS(ES)
Northwestern University
Evanston, IL 60208-1110

E-Mail: e-berns@northwestern.edu

8. PERFORMING ORGANIZATION REPORT NUMBER

9. SPONSORING / MONITORING AGENCY NAME(S) AND ADDRESS(ES)
U.S. Army Medical Research and Materiel Command
Fort Detrick, Maryland 21702-5012

10. SPONSORING / MONITORING AGENCY REPORT NUMBER

11. SUPPLEMENTARY NOTES

12a. DISTRIBUTION / AVAILABILITY STATEMENT
Approved for Public Release; Distribution Unlimited

12b. DISTRIBUTION CODE

13. ABSTRACT (Maximum 200 Words)

This final report presents progress achieved during a four year pre-doctoral traineeship project to determine the optimum techniques for a flat-panel Cesium-iodide silicon-diode full-field digital mammography system and to compare those optimized techniques to screen-film mammography at equal breast doses. This project work has analyzed the effect of technique factor selection (target-filtration, kVp, and mAs) on image contrast and low-contrast lesion detection under the conditions of matched average glandular dose to an optimized film-screen mammography system. Results indicate that low-contrast lesion detection was optimized for full-field digital mammography by using a softer x-ray beam for thin breasts and a harder x-ray beam for thick breasts. Under the constraint of matched average glandular dose between digital and screen-film mammography systems, optimum low-contrast lesion detection with full-field digital mammography was superior to that for screen-film mammography for all but the thinnest breasts. The results of this project have been published in two journal articles with another manuscript in preparation for submission and five abstracts have been published and presented at scientific meetings.

14. SUBJECT TERMS
breast imaging technology, full-field digital mammography, image quality, technique factors, quality control, quality assurance

15. NUMBER OF PAGES
71

16. PRICE CODE

17. SECURITY CLASSIFICATION OF REPORT	18. SECURITY CLASSIFICATION OF THIS PAGE	19. SECURITY CLASSIFICATION OF ABSTRACT	20. LIMITATION OF ABSTRACT
Unclassified	Unclassified	Unclassified	Unlimited

Table of Contents

Annual Summary Report

PI: R. Edward Hendrick, Ph.D. - Mentor
Eric A. Berns, Ph.D. – Pre-Doctoral Trainee

Introduction

The replacement of screen-film image receptors by full-field digital image receptors may increase the visibility of lesions, especially those within glandular tissues, by decoupling image acquisition and image display. Digital mammography systems permit user-adjustment of image display to maximize contrast resolution within specific tissues of interest. Thus, digital mammography has the potential to increase lesion visibility, especially improving the visibility of lesions in dense breasts, and the potential to decrease errors of perception and interpretation, again especially in dense breasts.

This project will optimize techniques to improve the detection and diagnosis of breast cancer using full-field digital mammography (FFDM) and compare them to screen-film mammography (SFM). If our hypotheses are correct, this study will result in optimized clinical techniques for mammography sites and provide a solution for an important and difficult area for current mammography: lesion detection in thicker, denser breasts. Finally, this study should provide and answer the question of how digital mammography compares to screen-film mammography in the detection of breast lesions.

The technical objectives of this study are to determine optimum techniques for a flat-panel Cesium-iodide silicon-diode full-field digital mammography system and to compare those optimized techniques to screen-film mammography at equal breast doses. Optimum techniques will be determined for the full range of compressed breast thicknesses and breast compositions. Optimization will be done by maximizing low-contrast lesion detectability in tissues of interest, especially glandular tissues, while keeping exposure times sufficiently short and mean glandular breast doses equal to those of screen-film mammography. The effect of full-field digital user-selectable technique

factors, including tube target material, filtration material, kVp setting, and mAs setting, on detector signal-to-noise ratios (SNR), contrast-to-noise ratios, low-contrast lesion detection, and radiation dose will be independently quantified. Once optimum technique factors for this full-field digital mammography system are obtained for each breast thickness and composition, those optimum techniques will be compared to optimum techniques for screen-film mammography under the constraint of equal average glandular breast doses.

Body

Two manuscripts came from this project. The first focused directly on the statement of work for this funded project. The second manuscript took the work a step further and compared optimized full-field digital mammography to screen-film mammography units in clinical practice. A third piece of work stemming from this project was to use the optimization results for full-field digital mammography (this study) and to test the effectiveness of Digital Subtraction Mammography (DSM) on phantoms. The research accomplishments are best described in the manuscripts contained in the appendices. Additionally, four abstracts were presented at scientific meetings.

Key Research Accomplishments

- Phantom testing was performed on the screen-film mammography unit to determine the optimized technique parameters.
- Optimized images of the contrast detail phantom were produced on the screen-film unit at 2, 4, 6, and 8 cm thicknesses. See Appendix A for image technique data.
- Medical physics testing was performed on the screen-film mammography unit to obtain data for calculation of average glandular dose. See Appendix B.
- Medical physics testing was performed on the GE Senographe 2000D full-field digital mammography unit to obtain data for calculation of average glandular doses. See Appendix B.

- A computer program was written to calculate average glandular dose for any set of technique factors on the digital mammography unit. An example output of the computer program is illustrated in Appendix C.
- A computer program was written to match the average glandular dose from one mammography machine to another machine by calculating the corresponding technique factors. An example output of the computer program is presented in Appendix D.
- Phantom images were acquired on the digital mammography unit using the calculated techniques that match the film-screen dose. See Appendix E.
- The phantom images acquired on the digital unit were printed and randomly scored by six trained individuals. The scores for each film were recorded for analysis. See Appendix F.
- Statistical analysis for the phantom image scores were analyzed to assess trends as a function of target-filter and kVp using a linear regression model. Two-sided t-tests were used to compare FFDM to SFM at each breast thickness (SAS Institute, Seattle, WA).
- A manuscript was written presenting the results from optimizing the full-field digital mammography system and abstracts were written and presented at several scientific meetings. See Appendices G, J, K, L, and M.
- A manuscript was written comparing optimized full-field digital mammography systems to screen-film mammography systems. See Appendix H.
- A manuscript was written presenting preliminary results for optimizing technique factors for full-field digital subtraction mammography. See Appendix I.

List of Reportable Outcomes

1. Manuscript published in March 2003 in Medical Physics titled "Optimization of technique factors for a silicon diode array full-field digital mammography system and comparison to screen-film mammography with matched average glandular dose". See Appendix G.

2. Manuscript published in May 2002 in Medical Physics titled "Performance comparison of full-field digital mammography to screen-film mammography in clinical practice". See Appendix H.
3. Preliminary manuscript to be submitted for publication in Medical Physics title "Optimizing and Selecting Technique Factors for Full-Field Digital Subtraction Mammography". See Appendix I.
4. Scientific presentation: Effect of Foam Pads On Mammography Dose Calculation. AAPM 2003. See Appendix J.
5. Scientific presentation: Optimization of Technique Factors for a Silicon Diode Array Full-Field Digital Mammography System and Comparison to Screen-Film Mammography with Matched Mean Glandular Dose. Era of Hope 2002 Department of Defense Breast Cancer Research Program Meeting, September 25-28, 2002. See Appendix K.
6. Scientific presentation: Clinical Performance Comparison of Full-Field Digital Mammography to Screen-Film Mammography. RSNA 2001. See Appendix L.
7. Scientific presentation: Optimization of technique factors for a silicon diode array full-field digital mammography system and comparison to screen-film mammography with matched mean glandular dose. RSNA 2001. See Appendix M.

Conclusions

Our results indicate that for a CsI scintillator and amorphous silicon detector, low-contrast lesion detection is maximized by using a softer x-ray beam (relatively low kVp) for thin breasts. Contrast-detail (CD) results for digital and screen-film mammography in thin breasts indicate that FFDM should not be expected to yield low-contrast lesion detection superior to that of SFM. Our results indicate that for 4 cm thick breasts, low-contrast lesion detection was insensitive to the target-filter and kVp selected between 25 and 35 kVp. For thick breasts (> 5 cm thick), on the other hand, low-contrast detection is maximized with this detector by selecting a harder x-ray beam. Our results indicated that at 6 cm, Rh-Rh at 30-35 kVp was optimum; at 8 cm, Rh-Rh at 40-46 kVp was optimum.

This is due to the combined effect of decreased breast absorption (and therefore decreased breast dose) for higher energy x-rays in thicker breasts and higher SNR per unit dose for higher energy x-rays. The use of a harder x-ray beam for thicker breasts has the added clinical benefit of increasing x-ray output, keeping exposure times short. This has been confirmed in a separate comparison of FFDM to SFM.[1] our CD results for 8 cm breasts indicate that Rh-Rh is preferable to the other two target-filter combinations. Our CD results indicate that higher kVp (up to 45 kVp) is preferable for thick breasts. These results indicate that low-contrast lesion detection is optimized for a CsI silicon diode array detector under the constraint of fixed breast dose by using a softer x-ray beam for thin breasts and a harder x-ray beam for thick breasts. Under this constraint, FFDM CD scores were superior to SFM CD scores for all but the thinnest breasts.

Results comparing exposure times and mean glandular doses for digital and screen-film mammography allay some possible concerns about the performance of digital mammography. For thicker breasts, where longer exposure times and higher breast doses are a potential concern, digital mammography performed better than screen-film mammography. Even for 8 cm breasts, where screen-film units yielded exposure times over 2 seconds (mean exposure time: 2.9 s), digital mammography consistently produced exposure times under 2 seconds (mean exposure time: 1.7 s). This reduction in exposure time is important in reducing motion artifacts on mammograms.

For 8 cm thick breasts, mean glandular doses averaged 3.05 milligray (mGy) for digital and 4.11 mGy for screen-film; 81% of screen-film units had doses higher than 3.05 mGy. At the same time, contrast-detail scores were higher for digital than for screen-film for 8 cm thick breasts.

Our results indicate that digital mammography had significantly reduced variances in exposure times and mean glandular doses, along with reduced variance in contrast-detail scores, compared to screen-film mammography at each breast thickness. Factors in the greater variability of screen-film image receptor sensitivities are the variability of system speed caused by the use of different screen-film combinations, different resultant film optical densities (ODs), and different film processing conditions. Digital detectors eliminate target OD variability and processing variability, substituting the variability of detector sensitivity in its place.

Digital mammography systems had similar exposure times and breast doses to screen-film mammography for thin to intermediate breasts, but resulted in shorter exposure times and lower mean glandular doses, on average, for thicker breasts. For all breast thicknesses, digital mammography had better detection of low-contrast simulated lesions, on average, than screen-film mammography. Digital mammography also demonstrated less variance than screen-film mammography in exposure times, mean glandular doses, and contrast-detail scores. These results indicate that clinical use of digital mammography may improve image quality for equal or lower breast doses, while providing tighter control over exposures and image quality than screen-film mammography.

Detailed descriptions of results and conclusions are presented in the two attached manuscripts (Appendix G & H) and four attached abstracts (Appendices J, K, L, and M).

References

1. Hendrick RE, Berns EA. Optimizing mammographic technique. In 1999 Syllabus: Categorical Course in Diagnostic Radiological Physics; Physical Aspects of Breast Imaging - Current and Future Considerations. AG Haus, MJ Yaffe, Editors. Oak Brook, IL: RSNA Publications, p. 79-89, 1999.

APPENDICES
A - M

Appendix A

Film-Screen Phantom Data

Date: 3/10/1999

	2 cm	4 cm	6 cm	8 cm
Target/Filter:	Mo/Mo	Mo/Mo	Mo/Rh	Rh/Rh
kVp:	25	25	27	28
mAs:	16	85	168	283
HVL:	0.3492	0.3429	0.4213	0.4315
Average Glandular Dose (mrad):	38.9	126.38	234.97	384.77
Optical Density:	1.56	1.66	1.58	1.59

Appendix B

Entrance Exposure Measurements

21-Jan-99

mAs = 100

kVp	DMR Mo/Mo	DMR Mo/Rh	DMR Rh/Rh	Digital Mo/Mo	Digital Mo/Rh	Digital Rh/Rh
22	542	417		503	378	
23	632	495		594	458	
24	733	586		694	547	
25	843	684	687	799	641	662
26	958	786	780	912	741	753
27	1083	893	881	1031	843	851
28	1211	1008	987	1156	952	955
29	1346	1125	1097	1286	1065	1063
30	1484	1245	1213	1419	1180	1175
31	1627	1367	1328	1559	1299	1292
32	1771	1492	1450	1701	1421	1412
33	1923	1623	1575	1846	1545	1536
34	2077	1755	1704	1998	1676	1664
35	2236	1894	1835	2152	1807	1796
36		2034	1971		1940	1930
37		2175	2111		2076	2067
38		2319	2252		2216	2207
39		2465	2395		2360	2347
40			2539		2501	2493
41			2688			2644
42			2840			2790
43			2990			2940
44			3150			3100
45			3290			3250
46			3450			3390
47			3610			3560
48			3770			3720
49						3880

HVL Measurements

21-Jan-99

kVp	DMR Mo/Mo	DMR Mo/Rh	DMR Rh/Rh	Digital Mo/Mo	Digital Mo/Rh	Digital Rh/Rh
22	0.3050	0.3425		0.3005	0.3352	
23	0.3153	0.3649		0.3105	0.3590	
24	0.3314	0.3819		0.3268	0.3775	
25	0.3429	0.3971	0.3804	0.3397	0.3938	0.3761
26	0.3540	0.4086	0.3984	0.3522	0.405	0.3938
27	0.3638	0.4213	0.4172	0.3617	0.4200	0.4122
28	0.3724	0.4303	0.4315	0.3712	0.4254	0.4274
29	0.3910	0.4393	0.4454	0.3877	0.4355	0.4413
30	0.3974	0.4478	0.4624	0.3958	0.4427	0.4585
31	0.4072	0.4612	0.4849	0.4007	0.4593	0.4794
32	0.4145	0.4714	0.4960	0.4098	0.4632	0.4916
33	0.4213	0.4744	0.5055	0.4178	0.4683	0.5049
34	0.4274	0.4787	0.5157	0.4229	0.4764	0.5139
35	0.4325	0.4813	0.5283	0.4294	0.4784	0.5281
36		0.4897	0.5358		0.4816	0.5354
37		0.4918	0.5470		0.4914	0.5423
38		0.4929	0.5549		0.4932	0.5535
39		0.4973	0.5557		0.4971	0.5578
40			0.5677		0.4997	0.5634
41			0.5678			0.5659
42			0.5753			0.5746
43			0.5809			0.5830
44			0.5866			0.5782
45			0.5922			0.5931
46			0.6012			0.6000
47			0.6098			0.6067
48			0.6160			0.6149
49						0.6199

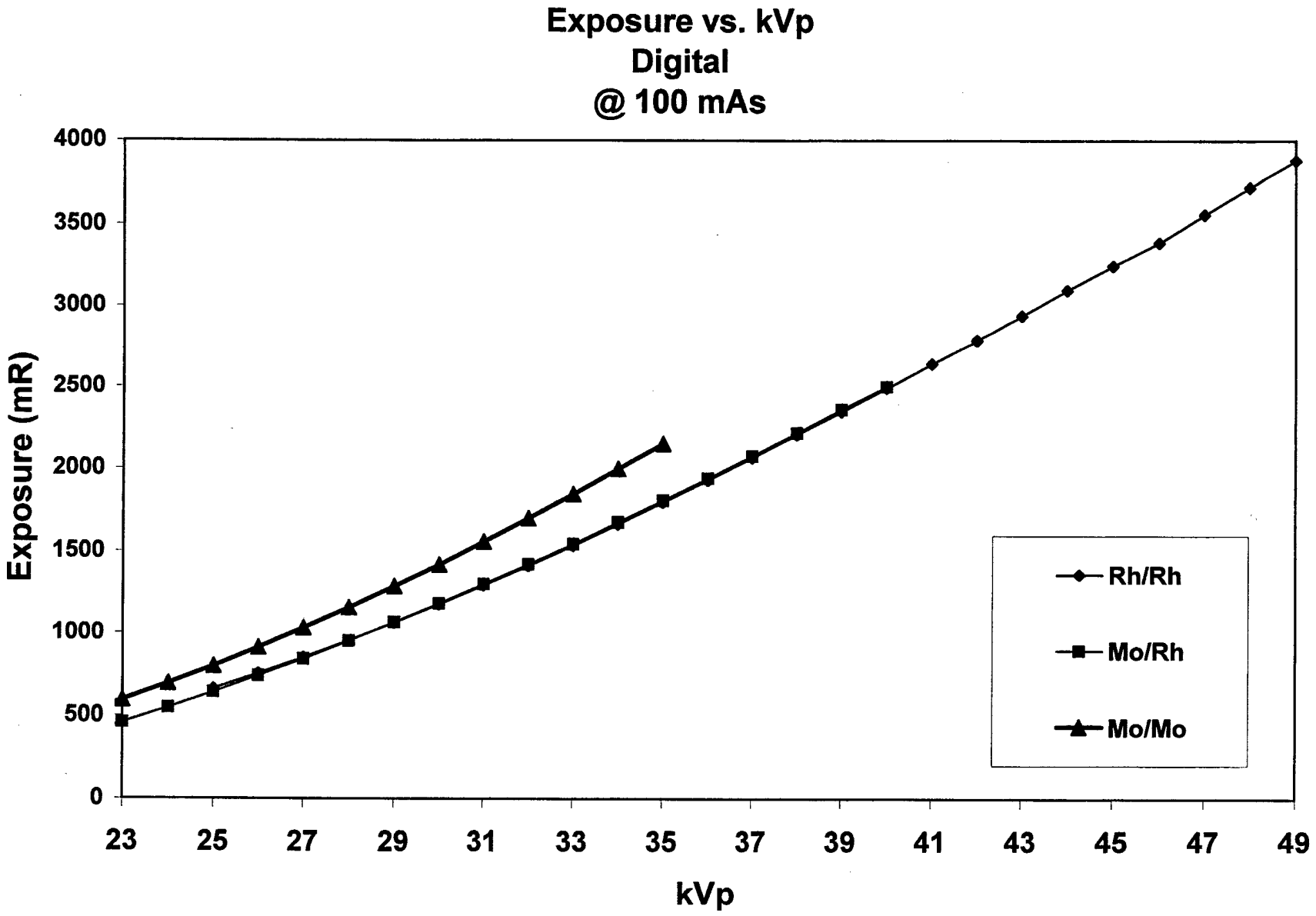
Exposure vs. kVp
Digital
@ 100 mAs
Exposure (mR)
4000
3500
3000
2500
2000
1500
1000
500
0
23
25
27
29
31
33
35
37
39
41
43
45
47
49
kVp
Rh/Rh
Mo/Rh
Mo/Mo

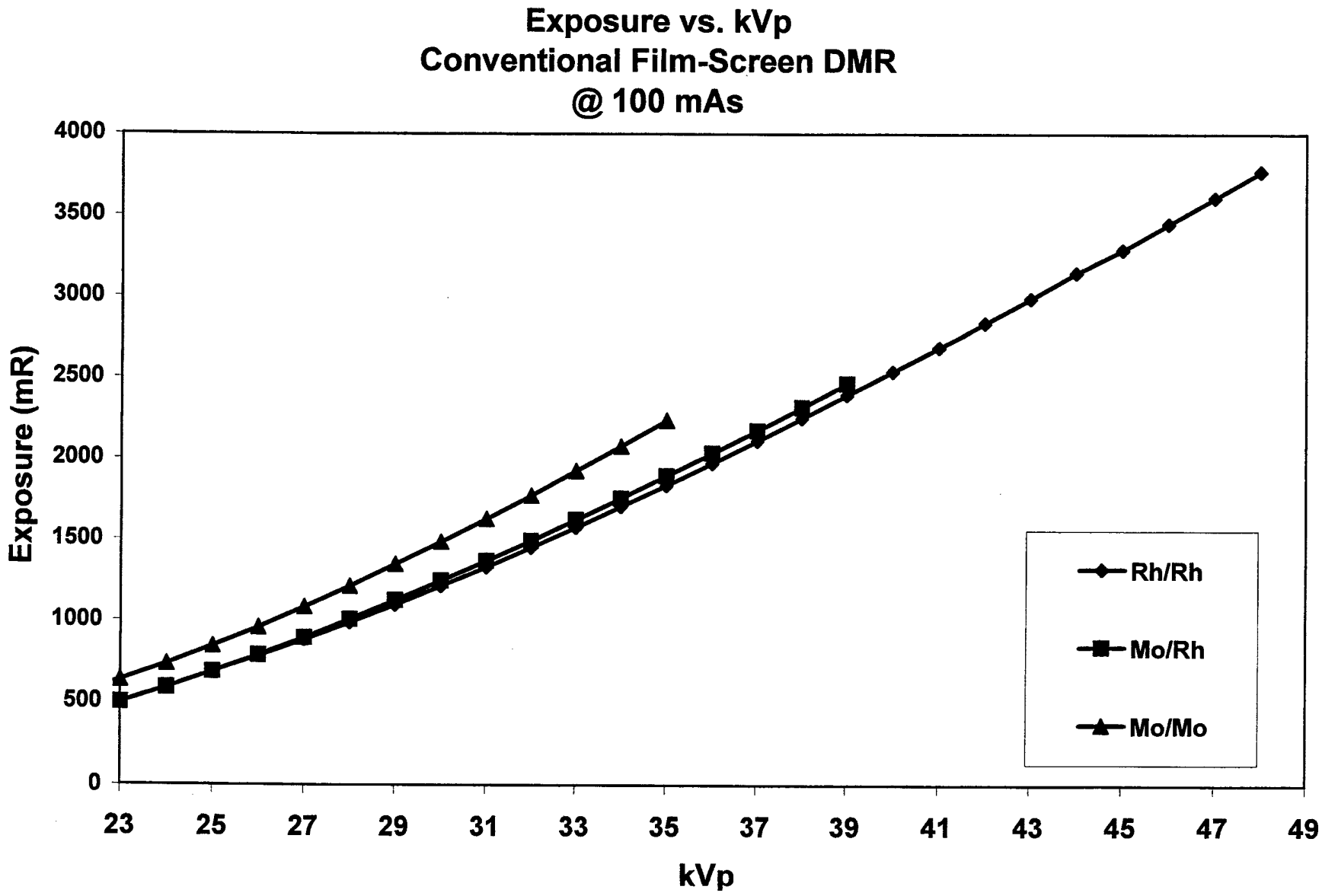
Exposure vs. kVp
Conventional Film-Screen DMR
@ 100 mAs
Exposure (mR)
4000
3500
3000
2500
2000
1500
1000
500
0
23
25
27
29
31
33
35
37
39
41
43
45
47
49
kVp
Rh/Rh
Mo/Rh
Mo/Mo

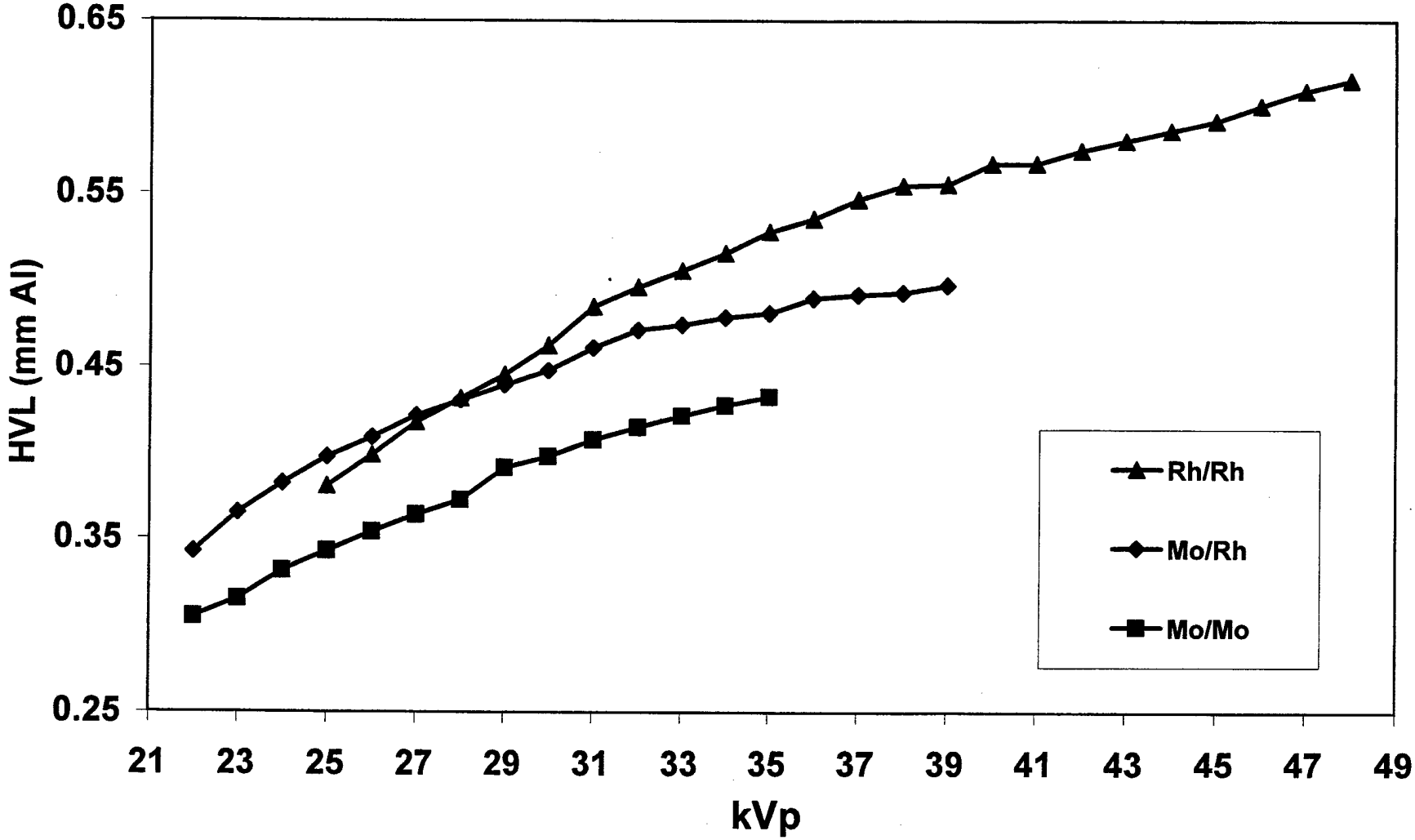
HVL vs. kVp
Conventional Film-Screen DMR
HVL (mm Al)
0.65
0.55
0.45
0.35
0.25
21
23
25
27
29
31
33
35
37
39
41
43
45
47
49
kVp
Rh/Rh
Mo/Rh
Mo/Mo

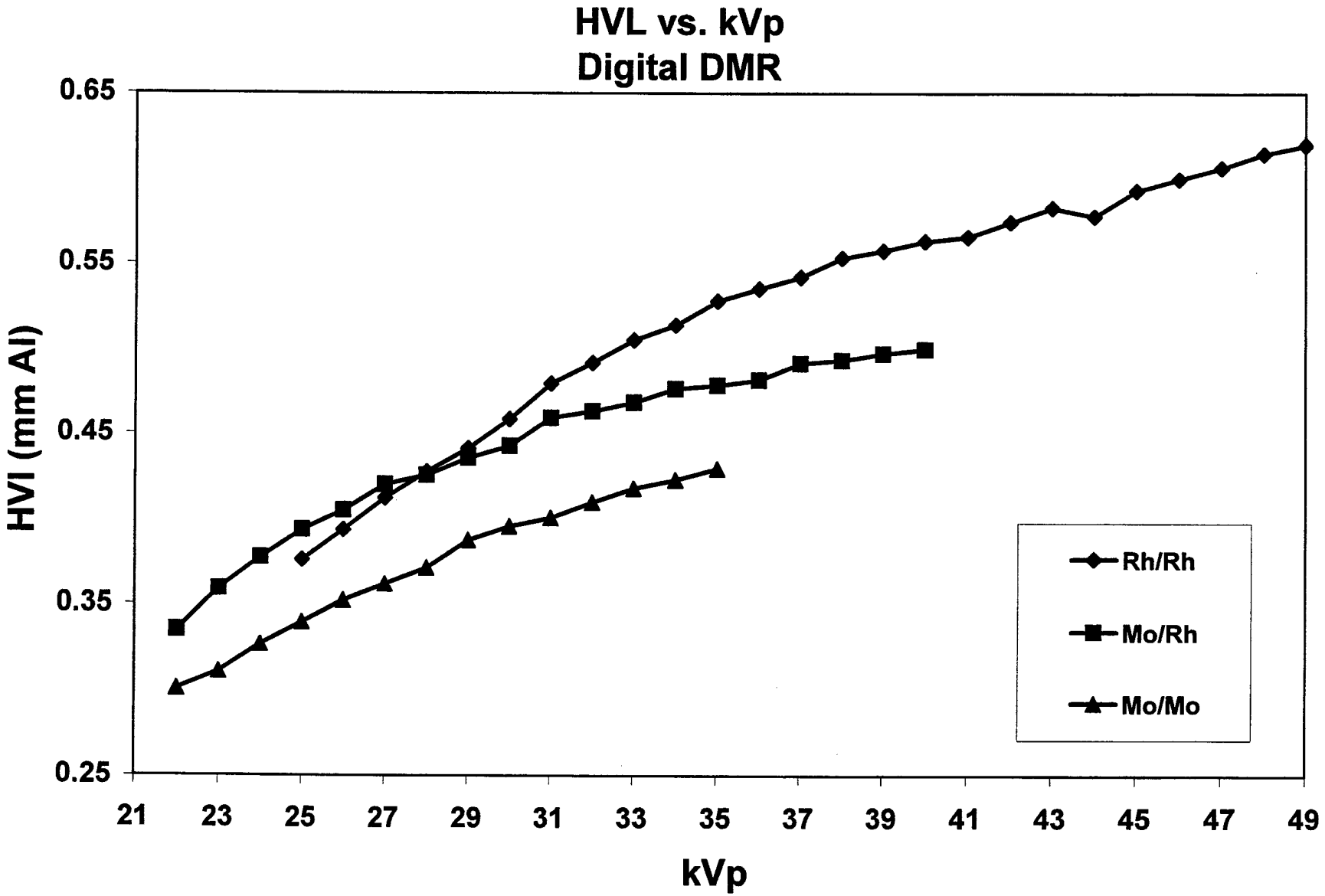
HVL vs. kVp
Digital DMR
HVl (mm Al)
0.65
0.55
0.45
0.35
0.25
21
23
25
27
29
31
33
35
37
39
41
43
45
47
49
kVp
Rh/Rh
Mo/Rh
Mo/Mo

Appendix C

Mammography Unit Dose Measurement Setup

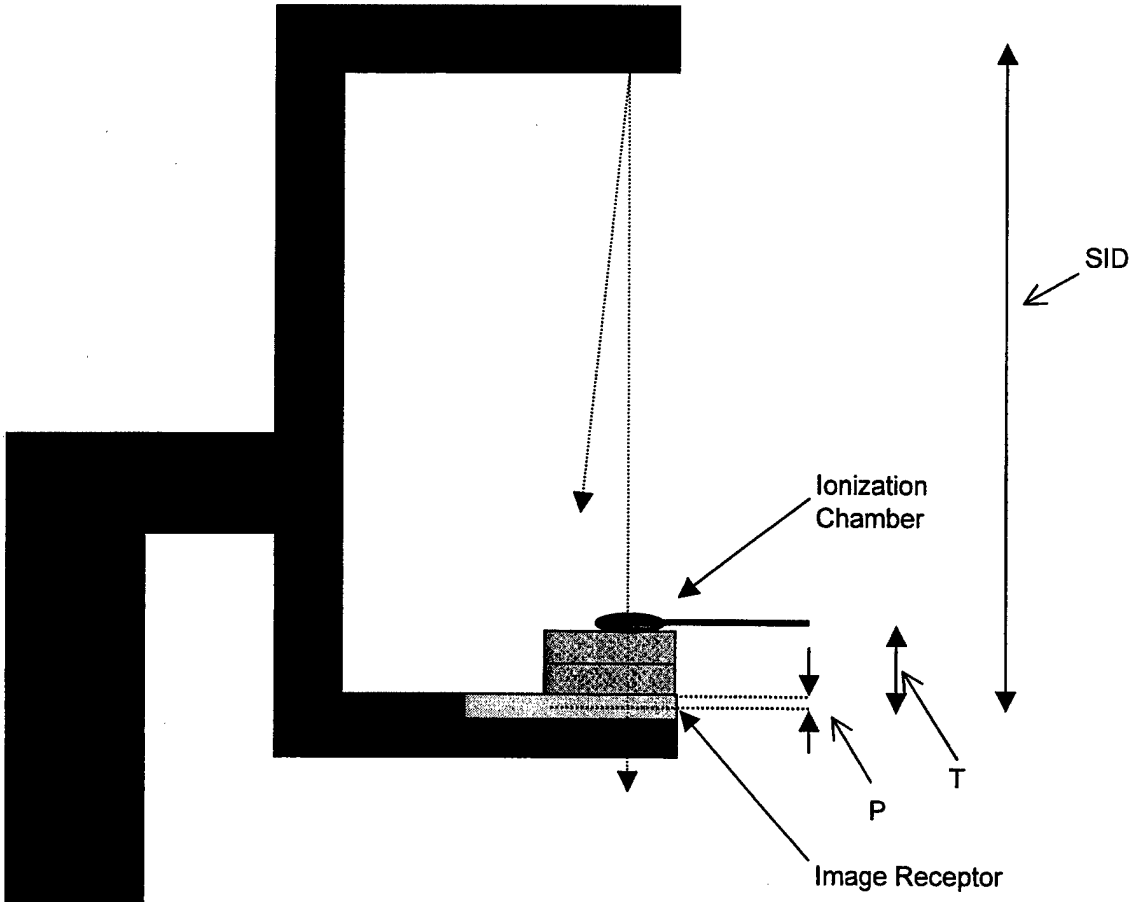

SID: Source to image receptor distance.

P: Distance between image receptor and breast support plate.

T: Thickness between breast support plate and center of ionization chamber.

Average Glandular Dose Calculation Program

Compressed Breast Thickness (mm)	42
Target/Filter (Mo/Mo, Mo/Rh, Rh/Rh)	Mo/Mo
kVp	26
Composition (100F, 50/50, 100G)	50/50
mAs	100
HVL (mm Al)	0.35
SSD (mm)	660
P(mm) = Distance from IR to Support Plate	16.85
Density Setting	0

D_{gN} (mrad/R)	175.5
Distance from support plate that entrance X measurements were made at (mm):	45
Entrance X at 45 mm from support plate	1000
mAs at 45 mm from support plate	100
mR/mAs at 45 mm from support plate	10.00
ESE - Entrance X (mR) at 42 mm from support plate at 100 mAs	990.04
AGD (mrad) = D_{gN} * ESE	**173.74**

DgN Calculation

Thickness (cm)	4.2
T/F (Mo/Mo, Mo/Rh, Rh/Rh)	Mo/Mo
kVp	26
Comp. (100F, 50/50, 100G)	50/50
HVL (mm Al)	0.35
D_{gN} (mrad/R)	175.5

	Mo/Mo 100% Fat	Mo/Mo 50/50	Mo/Mo 00% Gland.	Mo/Rh 100% Fat	Mo/Rh 50/50	Mo/Rh 00% Gland.	Rh/Rh 100% Fat	Rh/Rh 50/50	Rh/Rh 100% Gland.
a	10.43	7.40	5.56	13.61	9.63	7.22	9.54	6.12	4.22
b	5.36	5.15	4.88	5.60	5.44	5.23	5.73	5.63	5.43
c	0.53	0.59	0.62	0.52	0.59	0.64	0.57	0.68	0.76
u	147.43	140.27	122.87	119.29	130.02	118.76	94.41	129.64	124.24
v	6.99	7.02	7.02	6.86	6.89	6.91	6.86	6.87	6.90
w	0.24	0.31	0.37	0.20	0.28	0.34	0.17	0.25	0.31
D_{gN}	224.1	175.5	140.4	229.0	180.5	145.4	233.5	185.4	150.9

Concatenated T/F & Composition:	Mo/Mo	Mo/Rh	Rh/Rh
Mo/Mo50/50	175.5	xxx	xxx

Appendix D

Multiple Technique Dose Matching Program

3/25/2001

Patient:

Patient ID:

Date:

Film-Screen - Initial Technique

Comp. Breast Thickness (mm)	42
Target/Filter	Mo/Mo
kVp	26
Composition (100F, 50/50, 100G)	50/50
mAs	78
HVL (mm Al)	0.354
SSD (mm)	660
P(mm) = Dist. from IR to Support Plate	16.85
Density Setting	
D_{gN} (mrad/R)	177.2
Dist. from support plate to ion chamber (mm):	45
Ent. X at 45 mm from support plate	N/A
mAs at 45 mm from support plate	100
mR/mAs at 45 mm from support plate	9.58
Ent. X (mR) at 42 mm from support plate at 78 mAs	739.80
AGD (mrad) = D_{gN} * ESE	131.13

Digital - Matched Technique

Comp. Breast Thickness (mm)	42
Target/Filter	Mo/Mo
kVp	26
Composition (100F, 50/50, 100G)	50/50
mAs	**81.5**
HVL (mm Al)	0.3522
SSD (mm)	660
P(mm) = Dist. from IR to Support Plate	16.85
Density Setting	N/A
D_{gN} (mrad/R)	176.5
Dist. from support plate to ion chamber (mm):	45
Ent. X at 45 mm from support plate	N/A
mAs at 45 mm from support plate	100
mR/mAs at 45 mm from support plate	9.12
Ent. X (mR) at 42 mm from support plate at 81.4820056137612 mAs	735.72
AGD (mrad) = D_{gN} * ESE	131.13

	Mo/Mo	Mo/Rh	Rh/Rh
kVp	mAs	mAs	mAs
22	178.2	203.5	
23	144.7	157.3	
24	116.8	125.5	
25	96.9	102.9	100.8
26	81.5	86.6	84.6
27	69.9	73.5	71.3
28	60.7	64.2	60.9
29	52.3	56.1	52.7
30	46.4	49.8	45.7
31	41.7	43.7	39.7
32	37.4	39.6	35.4
33	33.7	36.0	31.8
34	30.7	32.7	28.9
35	28.0	30.2	26.4
36		27.9	24.5
37		25.5	22.8
38		23.8	21.2
39		22.0	20.0
40		20.5	18.7
41			17.6
42			16.4
43			15.2
44			14.3
45			13.1
46			12.1
47			11.1
48			10.2
49			9.4

Appendix E

Mammography Technique and Dose Matching Program

Patient:	2 cm
Patient ID#:	5010013
Date:	1/29/1999

DMR - Initial Technique

Thickness (cm)	2
T/F (Mo/Mo, Mo/Rh, Rh/Rh)	Mo/Mo
kVp	25
Comp.(100F, 50/50, 100G)	50/50
Entrance X (mR)	124.5
HVL (mm Al)	0.3429
Average Glandular Dose (mrad)	**38.88**
Density Setting	0
mAs	16
mR/mAs	7.78
mA	100
Exposure Time (sec.)	0.16
D_{gN} (mrad/R)	312.3

DIGITAL - Matched Technique

Thickness (cm)	2
T/F (Mo/Mo, Mo/Rh, Rh/Rh)	Mo/Mo
kVp	25
Comp.(100F, 50/50, 100G)	50/50
Entrance X (mR)	125.5
HVL (mm Al)	0.3397
Average Glandular Dose (mrad)	**38.88**
Density Setting	0
mAs	**17.0**
mR/mAs	7.38
mA	100
Exposure Time (sec.)	0.17
D_{gN} (mrad/R)	309.9

Digital DMR Matched Techniques

	Mo/Mo	Mo/Rh	Rh/Rh
kVp	mAs	mAs	mAs
22	30.3	35.7	
23	24.8	28.0	
24	20.3	22.5	
25	17.0	18.6	18.3
26	14.4	15.8	15.6
27	12.5	13.5	13.3
28	10.9	11.8	11.5
29	9.4	10.3	10.1
30	8.4	9.2	8.9
31	7.6	8.1	7.8
32	6.8	7.3	7.0
33	6.2	6.7	6.3
34	5.7	6.1	5.8
35	5.2	5.6	5.3
36		5.2	4.9
37		4.8	4.5
38		4.5	4.2
39		4.2	3.9
40		3.9	3.6
41			3.4
42			3.2
43			2.9
44			2.7
45			2.5
46			2.3
47			2.1
48			1.9
49			1.7

Mammography Technique and Dose Matching Program

Patient:	4 cm
Patient ID#:	5010014
Date:	1/29/1999

DMR - Initial Technique

Thickness (cm)	4
T/F (Mo/Mo, Mo/Rh, Rh/Rh)	Mo/Mo
kVp	25
Comp.(100F, 50/50, 100G)	50/50
Entrance X (mR)	705.0
HVL (mm Al)	0.3429
Average Glandular Dose (mrad)	**126.37**
Density Setting	0
mAs	85
mR/mAs	8.29
mA	100
Exposure Time (sec.)	0.85
D_{gN} (mrad/R)	179.3

DIGITAL - Matched Technique

Thickness (cm)	4
T/F (Mo/Mo, Mo/Rh, Rh/Rh)	Mo/Mo
kVp	25
Comp.(100F, 50/50, 100G)	50/50
Entrance X (mR)	710.9
HVL (mm Al)	0.3397
Average Glandular Dose (mrad)	**126.37**
Density Setting	0
mAs	**90.4**
mR/mAs	7.86
mA	100
Exposure Time (sec.)	0.90
D_{gN} (mrad/R)	177.8

Digital DMR Matched Techniques

	Mo/Mo	Mo/Rh	Rh/Rh
kVp	mAs	mAs	mAs
22	166.2	189.9	
23	134.9	146.9	
24	108.9	117.3	
25	90.4	96.3	94.5
26	76.1	81.0	79.3
27	65.3	68.9	66.9
28	56.7	60.1	57.2
29	48.9	52.5	49.5
30	43.4	46.7	43.0
31	39.0	41.0	37.4
32	35.0	37.2	33.3
33	31.6	33.8	29.9
34	28.8	30.7	27.3
35	26.3	28.3	24.8
36		26.2	23.0
37		24.0	21.5
38		22.4	20.0
39		20.8	18.8
40		19.4	17.6
41			16.6
42			15.4
43			14.3
44			13.5
45			12.3
46			11.4
47			10.5
48			9.6
49			8.8

Mammography Technique and Dose Matching Program

Patient:	6 cm
Patient ID#:	; & 5010016
Date:	1/29/1999

DMR - Initial Technique

Thickness (cm)	6
T/F (Mo/Mo, Mo/Rh, Rh/Rh)	Mo/Rh
kVp	27
Comp.(100F, 50/50, 100G)	50/50
Entrance X (mR)	1576.2
HVL (mm Al)	0.4213
Average Glandular Dose (mrad)	**234.97**
Density Setting	0
mAs	168
mR/mAs	9.38
mA	100
Exposure Time (sec.)	1.68
D_{gN} (mrad/R)	149.1

DIGITAL - Matched Technique

Thickness (cm)	6
T/F (Mo/Mo, Mo/Rh, Rh/Rh)	Mo/Rh
kVp	27
Comp.(100F, 50/50, 100G)	50/50
Entrance X (mR)	1580.5
HVL (mm Al)	0.42
Average Glandular Dose (mrad)	**234.97**
Density Setting	0
mAs	**178.5**
mR/mAs	8.86
mA	100
Exposure Time (sec.)	1.78
D_{gN} (mrad/R)	148.7

Digital DMR Matched Techniques

	Mo/Mo	Mo/Rh	Rh/Rh
kVp	mAs	mAs	mAs
22	444.7	508.7	
23	360.8	389.5	
24	290.6	308.7	
25	240.6	251.6	243.4
26	201.8	210.9	202.9
27	172.7	178.5	170.2
28	149.4	155.5	144.9
29	128.4	135.5	124.8
30	113.6	120.1	107.9
31	101.7	105.2	93.4
32	90.9	95.1	83.0
33	81.9	86.3	74.3
34	74.4	78.0	67.6
35	67.7	71.7	61.5
36		65.9	56.9
37		59.9	53.0
38		55.2	49.1
39		50.7	46.2
40		46.7	43.2
41			40.6
42			37.8
43			35.1
44			33.2
45			30.5
46			28.5
47			26.3
48			24.4
49			22.7

Mammography Technique and Dose Matching Program

Patient:	8 cm
Patient ID#:	5010018
Date:	1/29/1999

DMR - Initial Technique

Thickness (cm)	8
T/F (Mo/Mo, Mo/Rh, Rh/Rh)	Rh/Rh
kVp	28
Comp.(100F, 50/50, 100G)	50/50
Entrance X (mR)	3140.5
HVL (mm Al)	0.4315
Average Glandular Dose (mrad)	384.77
Density Setting	0
mAs	283
mR/mAs	11.10
mA	75
Exposure Time (sec.)	3.77
D_{gN} (mrad/R)	122.5

DIGITAL - Matched Technique

Thickness (cm)	8
T/F (Mo/Mo, Mo/Rh, Rh/Rh)	Rh/Rh
kVp	28
Comp.(100F, 50/50, 100G)	50/50
Entrance X (mR)	3166.8
HVL (mm Al)	0.4274
Average Glandular Dose (mrad)	384.77
Density Setting	0
mAs	294.9
mR/mAs	10.74
mA	75
Exposure Time (sec.)	3.93
D_{gN} (mrad/R)	121.5

Digital DMR Matched Techniques

	Mo/Mo	Mo/Rh	Rh/Rh
kVp	mAs	mAs	mAs
22	920.9	1062.0	
23	745.5	807.5	
24	599.9	636.9	
25	496.5	517.5	500.3
26	416.1	432.8	414.9
27	355.7	365.9	347.0
28	307.3	318.7	294.9
29	263.8	277.8	253.8
30	233.0	246.3	219.1
31	208.4	215.8	189.6
32	186.0	195.1	168.3
33	167.3	177.0	150.4
34	151.9	159.8	136.4
35	138.1	146.6	123.7
36		134.5	114.1
37		121.6	105.8
38		111.6	97.8
39		101.6	91.5
40		92.7	85.3
41			79.9
42			74.3
43			69.0
44			65.3
45			60.1
46			56.2
47			52.1
48			48.4
49			45.1

Appendix F

Contrast Detail Results

Thickness: **2 cm**

Date: 3/3/1999

Patient ID: 5010013

F/S Techniques:

T/F: Mo/Mo

kVp: 25

mAs: 16

hvl: 0.3429

AGD: 38.9 mrad

Film/ScreenCD Scores											
Jane	Ed	Eric	Brian	Lori	Julio	Min	Max	Mean	Std. Dev.	Count
13.610	13.609	14.806	12.754	13.606	14.100	12.75	14.81	13.75	0.68	6

Image #	HVL	kVp	mAs	Target/ Filter	Mean Signal	St. Dev.	SNR	FFDM CD Scores										
								Jane	Ed	Eric	Brian	Lori	Julio	Min	Max	Mean	Std. Dev.	Count
A47	0.3105	23	25	MoMo	756.42	10.92	69.27	14.038	13.748	14.176	12.320	13.318	13.105	12.32	14.18	13.45	0.69	6
A13	0.3522	26	14	MoMo	812.93	12.33	65.93	13.468	13.750	14.356	12.895	12.895	12.895	12.90	14.36	13.38	0.60	6
A70	0.3958	30	8	MoMo	864.01	15.14	57.07	13.043	13.043	13.749	12.470	12.898	13.321	12.47	13.75	13.09	0.43	6
A31	0.4229	34	5	MoMo	990.59	14.37	68.93	12.329	13.039	12.755	11.620	11.751	11.391	11.39	13.04	12.15	0.66	6
A71	0.359	23	28	MoRh	882.07	11.77	74.94	13.675	14.038	14.671	12.966	13.243	13.351	12.97	14.67	13.66	0.62	6
A20	0.405	26	16	MoRh	1005.51	13.71	73.34	12.904	11.411	13.609	11.466	13.039	13.464	11.41	13.61	12.65	0.97	6
A11	0.4427	30	9	MoRh	1024.53	16.01	63.99	12.474	12.760	13.325	11.188	11.749	12.049	11.19	13.33	12.26	0.76	6
A30	0.4784	35	5	MoRh	1109.76	14.8	74.98	12.755	13.320	12.755	12.041	13.039	12.470	12.04	13.32	12.73	0.44	6
A1	0.4997	40	4	MoRh	1253.19	15.91	78.77	12.045	12.755	12.614	10.124	12.896	11.680	10.12	12.90	12.02	1.04	6
A3	0.3761	25	18	RhRh	1047.23	13.73	76.27	13.895	13.820	13.963	12.541	13.963	14.069	12.54	14.07	13.71	0.58	6
A69	0.4413	29	10	RhRh	1259.22	17.95	70.15	13.324	13.040	13.183	11.188	12.753	12.895	11.19	13.32	12.73	0.78	6
A54	0.5049	33	6	RhRh	1367.24	19.14	71.43	12.194	11.469	13.114	11.046	12.331	11.751	11.05	13.11	11.98	0.73	6
A44	0.5423	37	4	RhRh	1517.03	18.03	84.14	13.039	12.614	13.181	9.845	12.259	11.894	9.85	13.18	12.14	1.22	6
				Min:	756.42	10.92	57.07	12.05	11.41	12.61	9.85	11.75	11.39					
				Max:	1517.03	19.14	84.14	14.04	14.04	14.67	12.97	13.96	14.07					
				mean:	1068.44	14.91	71.48	13.01	12.99	13.50	11.67	12.78	12.64					
				Std. Dev:	226.26	2.50	6.90	0.65	0.82	0.65	0.99	0.62	0.83					
				Count:	13.00	13.00	13.00	13.00	13.00	13.00	13.00	13.00	13.00					

Contrast Detail Results

Thickness: **4 cm** **Date:** 3/3/1999 **Patient ID:** 5010014

F/S Techniques:

T/F:	Mo/Mo	
kVp:	25	
mAs:	85	
hvl:	0.3429	
AGD:	126.38	mrad

Film/ScreenCD Scores										
Jane	Ed	Eric	Brian	Lori	Julio	Min	Max	Mean	Std. Dev.	Count
13.541	12.906	13.261	11.976	12.189	13.114	11.98	13.54	12.83	0.62	6

Image #	HVL	kVp	mAs	Target/ Filter	Mean Signal	St. Dev.	SNR	CD Scores Jane	Ed	Eric	Brian	Lori	Julio	Min	Max	Mean	Std. Dev.	Count
A9	0.6199	49	9	RhRh	3404.44	30.15	112.92	12.330	11.471	13.188	11.399	12.899	12.189	11.40	13.19	12.25	0.73	6
A29	0.583	43	14	RhRh	3132.47	29.16	107.42	13.393	13.963	13.391	11.678	13.391	13.783	11.68	13.96	13.27	0.82	6
A62	0.5535	38	20	RhRh	2646.92	26.1	101.41	13.825	14.383	14.381	12.611	13.958	13.675	12.61	14.38	13.81	0.65	6
A28	0.5139	34	28	RhRh	2314.41	25.23	91.73	13.824	13.614	14.389	12.616	14.210	13.786	12.62	14.39	13.74	0.62	6
A61	0.4413	29	50	RhRh	1968.16	21.47	91.67	14.499	14.389	14.813	13.044	14.775	14.638	13.04	14.81	14.36	0.66	6
A59	0.3938	26	80	RhRh	1696.35	19.24	88.17	15.238	14.106	14.249	12.333	13.120	14.958	12.33	15.24	14.00	1.10	6
A21	0.4971	39	20	MoRh	1868.27	20.12	92.86	13.470	13.329	13.891	11.333	13.459	13.748	11.33	13.89	13.21	0.94	6
A32	0.4784	35	28	MoRh	1663.31	18.4	90.40	13.966	15.096	15.236	13.039	14.389	14.529	13.04	15.24	14.38	0.80	6
A68	0.4427	30	45	MoRh	1441.18	16.8	85.78	14.393	14.668	14.950	12.480	12.325	12.753	12.33	14.95	13.59	1.20	6
A52	0.405	26	80	MoRh	1328.93	15.85	83.84	13.968	13.755	14.669	12.326	13.401	13.969	12.33	14.67	13.68	0.78	6
A53	0.359	23	140	MoRh	1083.65	14.07	77.02	14.220	14.318	15.195	12.406	14.311	14.171	12.41	15.20	14.10	0.91	6
A8	0.4229	34	28	MoMo	1395.41	16.78	83.16	14.251	13.893	14.315	12.613	12.760	10.900	10.90	14.32	13.12	1.31	6
A10	0.4007	31	40	MoMo	1316.77	15.93	82.66	13.828	13.830	14.671	12.120	13.961	13.036	12.12	14.67	13.57	0.88	6
A42	0.3712	28	56	MoMo	1129.75	15.03	75.17	13.954	14.530	14.523	12.899	13.671	14.385	12.90	14.53	13.99	0.64	6
A23	0.3005	22	160	MoMo	772.32	11.85	65.17	14.174	13.963	14.171	12.259	13.610	13.608	12.26	14.17	13.63	0.72	6
A22	0.3268	24	110	MoMo	950.21	13.17	72.15	14.173	14.731	14.943	12.471	14.589	14.309	12.47	14.94	14.20	0.89	6
				Min:	772.32	11.85	65.17	12.33	11.47	13.19	11.33	12.33	10.90					
				Max:	3404.44	30.15	112.92	15.24	15.10	15.24	13.04	14.78	14.96					
				mean:	1757.03	19.33	87.60	13.97	14.00	14.44	12.35	13.68	13.65					
				Std. Dev:	768.24	5.64	12.55	0.61	0.82	0.58	0.51	0.69	1.02					
				Count:	16.00	16.00	16.00	16.00	16.00	16.00	16.00	16.00	16.00					

Contrast Detail Results

Thickness: **6 cm** **Date:** 06/16/99 **Patient ID:** 5010015 & 5010016

F/S Techniques:

T/F:	Mo/Rh
kVp:	27
mAs:	168
hvl:	0.4213
AGD:	234.97 mrad

Film/ScreenCD Scores										
Jane	Ed	Eric	Brian	Lori	Julio	Min	Max	Mean	Std. Dev.	Count
11.045	11.696	11.765	10.626	10.903	11.620	10.63	11.77	11.28	0.48	6

Image #	HVL	kVp	mAs	Target/ Filter	Mean Signal	St. Dev.	SNR	CD Scores Jane	Ed	Eric	Brian	Lori	Julio	Min	Max	Mean	Std. Dev.	Count
A64	0.6199	49	22.5	RhRh	3973.69	33.91	117.18	12.824	13.824	12.824	12.116	13.114	12.824	12.12	13.82	12.92	0.55	6
A49	0.6	46	28	RhRh	3696.65	31.11	118.83	13.255	13.248	13.108	12.470	12.750	13.108	12.47	13.26	12.99	0.31	6
A24	0.5782	44	32	RhRh	3417.07	30.08	113.60	13.614	13.189	12.754	11.328	13.176	13.179	11.33	13.61	12.87	0.80	6
A26	0.5659	41	40	RhRh	3019.11	28.83	104.72	12.894	13.039	13.390	12.400	12.613	12.895	12.40	13.39	12.87	0.34	6
A72	0.5535	38	56	RhRh	2571.07	25.67	100.16	12.965	13.614	13.108	12.188	12.188	12.825	12.19	13.61	12.81	0.55	6
A14	0.5281	35	63	RhRh	2158.91	24.06	89.73	13.683	13.968	13.398	11.909	12.903	13.506	11.91	13.97	13.23	0.74	6
A56	0.4916	32	80	RhRh	1764.92	21.29	82.90	13.041	13.331	13.181	11.344	13.039	13.181	11.34	13.33	12.85	0.75	6
A51	0.4585	30	110	RhRh	1742.91	21.26	81.98	13.185	13.755	13.326	12.683	13.185	13.750	12.68	13.76	13.31	0.40	6
A46	0.4274	28	140	RhRh	1506.68	19.38	77.74	12.753	13.331	12.470	11.764	13.331	13.185	11.76	13.33	12.81	0.62	6
A16	0.3939	26	200	RhRh	1347.95	18.05	74.68	13.044	14.171	13.181	12.609	13.181	13.173	12.61	14.17	13.23	0.51	6
A19	0.4997	40	45	MoRh	1895.64	20.55	92.25	12.031	12.898	12.613	11.900	12.048	12.754	11.90	12.90	12.37	0.43	6
A63	0.4849	36	63	MoRh	1515.25	18.99	79.79	12.189	12.620	12.616	11.768	13.464	13.604	11.77	13.60	12.71	0.71	6
A76	0.4764	34	80	MoRh	1449.31	18.69	77.54	11.894	13.826	12.474	12.189	12.616	12.966	11.89	13.83	12.66	0.68	6
A73	0.4427	30	125	MoRh	1261.74	17.84	70.73	12.338	13.476	12.330	11.340	13.318	13.176	11.34	13.48	12.66	0.81	6
A45	0.42	27	180	MoRh	1081.66	16.44	65.79	12.466	13.039	12.821	11.906	12.899	13.111	11.91	13.11	12.71	0.45	6
A15	0.3938	25	250	MoRh	986.23	17.52	56.29	12.188	12.620	12.471	11.764	12.611	13.033	11.76	13.03	12.45	0.43	6
A33	0.3352	22	500	MoRh	682.53	12.83	53.20	12.189	13.111	11.754	11.619	12.544	12.826	11.62	13.11	12.34	0.59	6
A78	0.4294	35	63	MoMo	1261.37	17.08	73.85	11.905	13.119	11.908	11.200	11.478	11.623	11.20	13.12	11.87	0.67	6
A79	0.4178	33	80	MoMo	1161.2	17.48	66.43	11.913	12.759	11.896	9.994	12.036	12.036	9.99	12.76	11.77	0.93	6
A39	0.4007	31	100	MoMo	1028.79	15.08	68.22	12.188	12.194	12.191	11.621	12.624	12.475	11.62	12.62	12.22	0.34	6
A2	0.3877	29	125	MoMo	880.73	15.36	57.34	11.325	13.184	12.611	11.335	12.321	12.466	11.33	13.18	12.21	0.74	6
A60	0.3522	26	200	MoMo	726.16	13.79	52.66	12.050	13.043	12.114	12.256	12.893	12.614	12.05	13.04	12.50	0.42	6
A36	0.3268	24	280	MoMo	604.2	12.23	49.40	12.193	12.761	12.046	10.919	12.754	12.966	10.92	12.97	12.27	0.75	6
A38	0.3005	22	450	MoMo	519.4	12.36	42.02	11.488	12.340	12.194	10.415	11.625	12.478	10.42	12.48	11.76	0.77	6
				Min:	519.40	12.23	42.02	11.33	12.19	11.75	9.99	11.48	11.62					
				Max:	3973.69	33.91	118.83	13.68	14.17	13.40	12.68	13.46	13.75					
				mean:	1677.22	20.00	77.79	12.48	13.19	12.62	11.71	12.70	12.91					
				Std. Dev:	986.22	6.07	21.65	0.63	0.51	0.50	0.66	0.53	0.47					
				Count:	24.00	24.00	24.00	24.00	24.00	24.00	24.00	24.00	24.00					

Contrast Detail Results

Thickness: **8 cm**

Date: 10/08/99 **Patient ID:** 5010018

F/S Techniques:

T/F:	Rh/Rh
kVp:	28
mAs:	283
hvl:	0.4315
AGD:	384.77 mrad

Film/ScreenCD Scores										
Jane	Ed	Eric	Brian	Lori	Julio	Min	Max	Mean	Std. Dev.	Count
8.859	10.206	10.704	8.859	8.294	9.986	8.29	10.70	9.48	0.94	6

Image #	HVL	kVp	mAs	Target/ Filter	Mean Signal	St. Dev.	SNR	CD Scores Jane	Ed	Eric	Brian	Lori	Julio	Min	Max	Mean	Std. Dev.	Count
A7	0.6199	49	45	RhRh	4048.43	33.22	121.87	11.623	12.759	13.044	10.833	12.754	12.329	10.83	13.04	12.22	0.84	6
A4	0.6	46	56	RhRh	3616.57	30.3	119.36	12.626	13.191	12.906	12.556	12.616	13.183	12.56	13.19	12.85	0.29	6
A65	0.583	43	71	RhRh	3152.01	28.15	111.97	12.051	12.623	13.330	11.619	12.609	13.181	11.62	13.33	12.57	0.65	6
A57	0.5578	39	90	RhRh	2259.47	22.88	98.75	11.770	13.119	12.684	11.629	12.616	12.971	11.63	13.12	12.46	0.62	6
A40	0.3532	36	110	RhRh	1737.29	20.49	84.79	10.913	13.326	12.549	10.913	12.899	12.690	10.91	13.33	12.22	1.04	6
A37	0.5139	34	140	RhRh	1605.5	19.86	80.84	11.184	13.609	12.906	10.338	12.606	12.469	10.34	13.61	12.19	1.20	6
A12	0.4413	29	250	RhRh	1168.95	17.08	68.44	11.346	11.914	11.770	11.063	12.400	12.188	11.06	12.40	11.78	0.50	6
A6	0.3761	25	500	RhRh	849.42	14.77	57.51	10.625	12.408	11.908	10.779	12.118	11.480	10.63	12.41	11.55	0.73	6
A17	0.4997	40	90	MoRh	1684.08	20.04	84.04	9.853	10.928	9.788	9.706	10.408	11.133	9.71	11.13	10.30	0.62	6
A58	0.4914	37	125	MoRh	1416.49	18.22	77.74	10.625	12.475	11.341	11.059	12.400	12.613	10.63	12.61	11.75	0.85	6
A55	0.4764	34	160	MoRh	1087.74	15.76	69.02	8.515	10.976	10.126	9.428	9.628	10.265	8.52	10.98	9.82	0.84	6
A35	0.4632	32	200	MoRh	973.72	15.18	64.14	10.061	11.486	10.776	8.438	11.344	11.626	8.44	11.63	10.62	1.22	6
A25	0.4355	29	288	MoRh	800.97	13.81	58.00	9.710	11.848	11.703	9.573	11.260	11.130	9.57	11.85	10.87	0.99	6
A48	0.42	27	360	MoRh	690.99	13.82	50.00	8.385	11.779	11.544	8.103	12.760	12.336	8.10	12.76	10.82	2.04	6
A80	0.3775	24	600	MoRh	544.99	12.1	45.04	8.935	10.428	11.500	9.993	11.685	10.573	8.94	11.69	10.52	1.01	6
A74	0.4294	35	140	MoMo	1118.86	16.28	68.73	9.075	11.568	9.781	9.144	9.926	10.641	9.08	11.57	10.02	0.95	6
A67	0.4178	33	160	MoMo	864.53	14.24	60.71	8.378	10.708	9.790	9.845	10.495	8.865	8.38	10.71	9.68	0.91	6
A27	0.3958	30	225	MoMo	650.67	12.77	50.95	7.813	10.223	9.433	7.385	8.513	9.433	7.39	10.22	8.80	1.08	6
A50	0.3617	27	360	MoMo	498.63	11.88	41.97	7.243	10.290	9.436	8.585	9.286	10.641	7.24	10.64	9.25	1.23	6
A5	0.3268	24	600	MoMo	346.72	8.78	39.49	6.410	10.223	9.015	6.410	8.935	8.660	6.41	10.22	8.28	1.54	6
				Min:	346.72	8.78	39.49	6.41	10.22	9.02	6.41	8.51	8.66					
				Max:	4048.43	33.22	121.87	12.63	13.61	13.33	12.56	12.90	13.18					
				mean:	1455.80	17.98	72.67	9.86	11.79	11.27	9.87	11.36	11.42					
				Std. Dev:	1051.01	6.43	24.81	1.72	1.12	1.40	1.54	1.46	1.39					
				Count:	20.00	20.00	20.00	20.00	20.00	20.00	20.00	20.00	20.00					

Appendix G

Optimization of technique factors for a silicon diode array full-field digital mammography system and comparison to screen-film mammography with matched average glandular dose

Eric A. Berns[a] and R. Edward Hendrick
The Lynn Sage Comprehensive Breast Center, Northwestern University Medical School, Chicago, Illinois 60611

Gary R. Cutter
Center for Research Design and Statistical Methods, University of Nevada, Reno, Nevada

(Received 14 May 2002; accepted for publication 16 December 2002; published 5 February 2003)

Contrast-detail experiments were performed to optimize technique factors for the detection of low-contrast lesions using a silicon diode array full-field digital mammography (FFDM) system under the conditions of a matched average glandular dose (AGD) for different techniques. Optimization was performed for compressed breast thickness from 2 to 8 cm. FFDM results were compared to screen-film mammography (SFM) at each breast thickness. Four contrast-detail (CD) images were acquired on a SFM unit with optimal techniques at 2, 4, 6, and 8 cm breast thicknesses. The AGD for each breast thickness was calculated based on half-value layer (HVL) and entrance exposure measurements on the SFM unit. A computer algorithm was developed and used to determine FFDM beam current (mAs) that matched AGD between FFDM and SFM at each thickness, while varying target, filter, and peak kilovoltage (kVp) across the full range available for the FFDM unit. CD images were then acquired on FFDM for kVp values from 23–35 for a molybdenum–molybdenum (Mo–Mo), 23–40 for a molybdenum–rhodium (Mo–Rh), and 25–49 for a rhodium–rhodium (Rh–Rh) target-filter under the constraint of matching the AGD from screen-film for each breast thickness (2, 4, 6, and 8 cm). CD images were scored independently for SFM and each FFDM technique by six readers. CD scores were analyzed to assess trends as a function of target–filter and kVp and were compared to SFM at each breast thickness. For 2 cm thick breasts, optimal FFDM CD scores occurred at the lowest possible kVp setting for each target–filter, with significant decreases in FFDM CD scores as kVp was increased under the constraint of matched AGD. For 2 cm breasts, optimal FFDM CD scores were not significantly different from SFM CD scores. For 4–8 cm breasts, optimum FFDM CD scores were superior to SFM CD scores. For 4 cm breasts, FFDM CD scores decreased as kVp increased for each target–filter combination. For 6 cm breasts, CD scores decreased slightly as kVp increased for Mo–Mo, but did not change significantly as a function of kVp for either Mo–Rh or Rh–Rh. For 8 cm breasts, Rh/Rh FFDM CD scores were superior to other target–filter combinations and increased significantly as kVp increased. These results indicate that low-contrast lesion detection was optimized for FFDM by using a softer x-ray beam for thin breasts and a harder x-ray beam for thick breasts, when AGD was kept constant for a given breast thickness. Under this constraint, optimum low-contrast lesion detection with FFDM was superior to that for SFM for all but the thinnest breasts. [DOI: 10.1118/1.1544674]

I. INTRODUCTION

Screening mammography trials have shown that mammography has a sensitivity to breast cancer ranging from 60% to 90%, with a trend toward lower sensitivity in premenopausal women.[1,2] Several independent analyses have shown that missed breast cancers are more likely to occur in radiographically dense breasts.[3–5] It is known that radiographically denser breasts have a greater probability of masking breast cancers, due to the similar x-ray attenuation properties of glandular tissues and breast cancers. The higher the glandular content of the breast, the greater the probability that breast cancer will be obscured by fibroglandular tissues.

The replacement of screen-film image receptors by full-field digital image receptors may increase the visibility of lesions, especially those within glandular tissues, by decoupling image acquisition and image display. Digital mammography eliminates the adverse effects of the characteristic curve, which reduces contrast in underexposed or overexposed screen-film images. Thus, in digital mammography adequate contrast resolution should exist among all breast tissues, as long as signal-to-noise ratios are adequate, since digital mammography permits user adjustment of image display to maximize contrast resolution within specific tissues of interest. Thus, digital mammography has the potential to increase lesion visibility, especially improving the visibility of lesions in dense breasts, and the potential to decrease errors of perception and interpretation. Preliminary studies of small-field and prototype full-field digital image receptors using contrast-detail phantoms suggest that digital mam-

mography will offer improved low-contrast resolution capabilities.[6]

There have been only a few published studies evaluating the influence of technique factors on low-contrast lesion detection with full-field digital mammography. Previous work has been done using an energy transport model to optimize spectral shape for a digital detector using a Gd_2O_2S scintillating screen coupled to a solid state CCD photodetector.[7] That work found that improvements in signal-to-noise ratios can be made by choosing different target materials for different breast thicknesses. Another study evaluated optimized technique parameters for a slot-scanning digital mammography system and suggested that optimization can maximize image quality and that each system be individually optimized.[8] Dance *et al.*, used measured spectra and Monte Carlo simulations to determine the effect of target–filter and tube potential on contrast, signal-to-noise ratios, and average absorbed doses in both screen-film and generic digital mammography.[9] Huda *et al.* modeled signal-to-noise ratios and breast dose as a function of photon energy in mammography using a figure of merit and assuming a monoenergetic x-ray beam.[10] The results of these previous studies are relevant to our study, but measurements were made on different detector types or simulations were made for more generic digital systems, not for the cesium-iodide silicon diode array used in this study.

Williams *et al.* evaluated the cesium-iodide amorphous silicon detector, along with two other digital mammography detectors, by using a "figure of merit" (FOM) as a metric for image quality.[11] In their work, FOM was defined as FOM $=SNR^2/AGD$, where AGD is the average glandular breast dose. Another metric used in the work was to measure the contrast-to-noise ratio across a slab of glandular tissue and calcified tissue relative to a uniform background. These measurements were taken for 3, 5, and 7 cm thick tissue-equivalent phantoms under manual exposures under the condition of an approximately matched detector signal.

In this paper, we determined optimized technique factors for the detection of low-contrast lesions using a silicon diode array full-field digital mammography (FFDM) system. FFDM AGD was matched to the AGD for screen-film mammography at each of four breast thicknesses: 2, 4, 6, and 8 cm. Then, as the target–filter and kVp were varied, FFDM AGD was kept constant for a given breast thickness. We compared FFDM results to screen-film mammography (SFM) results for low-contrast detection at each breast thickness. This paper differs from the previously cited paper by using the detection of simulated low-contrast lesions as the detection task and we perform this task under the condition of matched AGD to the breast, not matched signal to the detector.[11]

II. MATERIALS AND METHODS

Four contrast-detail (CD) images were acquired at 2, 4, 6, and 8 cm breast thicknesses on a SFM unit with optimized techniques using the optimization method described by Hendrick *et al.*, with target optical densities in the range of 1.55–1.70.[12] A D-shaped uniform CD phantom made of 1 cm slabs of tissue-equivalent material was used, one section of which contained a 9×9 contrast-detail pattern for the assessment of simulated low-contrast lesions (Fig. 1). The contrast-detail phantom was made from tissue-equivalent material designed to simulate 50% glandular/50% fatty breast tissues (BR 50/50). The phantom was the prototype for a digital mammography phantom offered commercially (Model 082, Computerized Imaging Reference Systems, Inc.), but has slightly different contrast specifications. Contrast was produced by circular holes drilled into the BR 50/50 breast equivalent material at diameters of 0.25, 0.5, 0.75, 1.0, 1.5, 2.0, 2.5, 3.0, and 4.0 mm. Each hole diameter was drilled at nine different depths of 0.05, 0.1, 0.15, 0.2, 0.3, 0.4, 0.5, 0.6, and 0.7 mm, yielding a square array of 81 objects. Each D-shaped slab was a semicircular phantom 18 cm in diameter and 1 cm thick. One D-shaped slab contained the contrast-detail pattern; the remainder were identical in shape but of uniform thickness and composition.

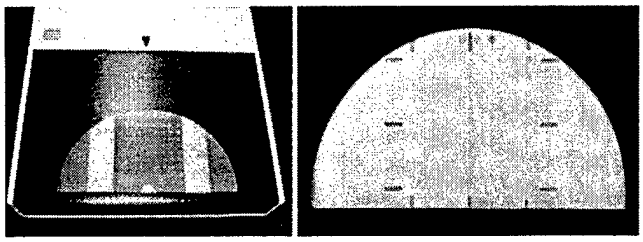

FIG. 1. Contrast-detail phantom on image receptor (left) and an x-ray image of the contrast-detail phantom (right).

Technique factors were recorded for each CD image and the corresponding AGD was calculated for each phantom thickness using HVL and entrance exposure measurements made on the SFM unit.[13,14]

To calculate techniques for the FFDM unit, a computer program was developed to determine the mAs value that gave an equal average glandular dose at each target–filter and kVp combination for each breast thickness. Half-value layer (HVL) and entrance exposure measurements were made on both the SFM unit and the FFDM unit at each target–filter and kVp to calculate AGD. The computer program was written to take into account any change in system performance (output or beam quality) and calculate the exact techniques needed to produce the desired average glandular dose.

CD images were then acquired on the FFDM unit using manual techniques for kVp values from 23–35 for Mo–Mo, 23–40 kVp for Mo–Rh, and 25–49 kVp for Rh–Rh, under the constraint of keeping AGD constant for a given breast thickness. mAs values were chosen to provide the matched AGD and images were acquired at approximately every second or third kVp step on the FFDM unit.

Screen-film CD images were scored by six readers under standardized viewing conditions. These included complete masking of each CD image and low ambient room lighting (<10 lux). Scoring of the CD phantom was done in a standardized manner, starting with the highest-contrast row of

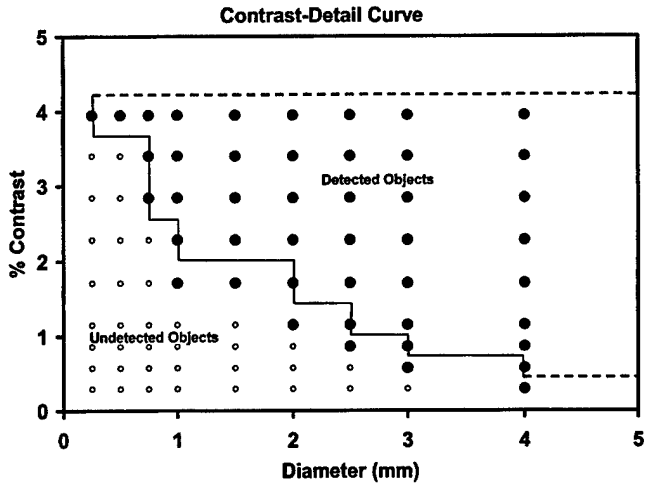

FIG. 2. Schematic of contrast-detail area score calculation. The CD score was defined as the product of the percent contrast and diameter area, including all detected objects.

objects, reading from the largest to smallest detectable object diameter in that row. An object was judged as "detected" if it occurred in the correct location, appeared generally round, and was more visible than artifactual "objects" occurring in the background of the CD phantom, excluding the locations of the 81 test objects. This comparison of detected objects against artifacts in the background of the phantom, similar to the method developed for scoring the ACR mammography accreditation phantom, was used to guard against overscoring due to prior knowledge of the location of the test objects in the phantom. Once an object was deemed too faint to detect, was not generally round, or was less conspicuous than artifacts in the background of the phantom, counting was stopped and the number of consecutively visible objects in that row was recorded. The reviewer then moved on to the next row of objects at slightly lower contrast, repeating the procedure. The CD score of each image was determined by calculating the area of detected objects in CD space (Fig. 2). The more low-contrast objects detected, the higher the CD score. If no objects were detected, a minimum score of zero would result; if all 81 objects were detected, a maximum score of 17.34 would result.

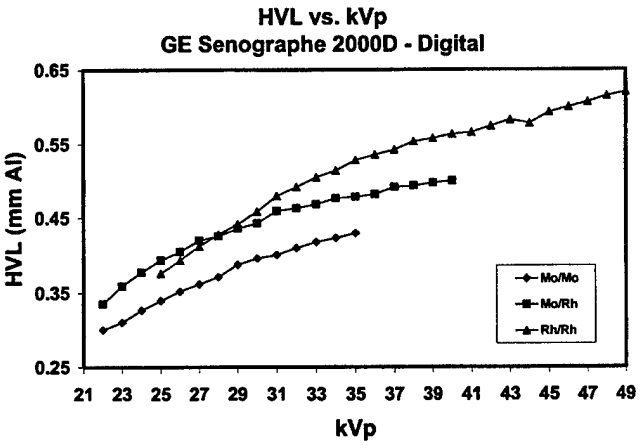

FIG. 4. HVL vs kVp results for the GE Senographe 2000D full-field digital mammography unit.

FFDM CD images were scored by the same six readers on the GE Review Workstation under optimized viewing conditions using the same scoring methods described above. Results were analyzed for statistical significance using analysis of variance methods (SAS Institute, Seattle, WA). CD scores were analyzed to assess trends as a function of target–filter and kVp using the general linear model (PROC GLM). Two-sided t tests were used to compare FFDM to SFM at each breast thickness (PROC T-TEST).[15]

III. RESULTS

Results of HVL measurements for the dose matching computer program are shown in Figs. 3 and 4 for both the GE DMR SFM unit and the GE Senographe 2000D FFDM unit. As expected, measured HVLs increased as kVp increased for each target–filter combination. HVL measurements were consistent between the SFM unit and FFDM unit, with HVL's ranging from 0.30 to 0.43 mm Al for Mo/Mo, 0.34 to 0.50 for Mo/Rh, and 0.38 to 0.62 for Rh/Rh.

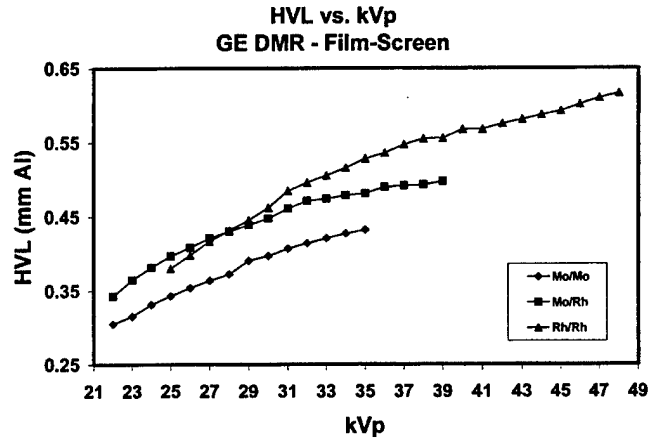

FIG. 3. HVL vs kVp results for the GE DMR screen-film unit.

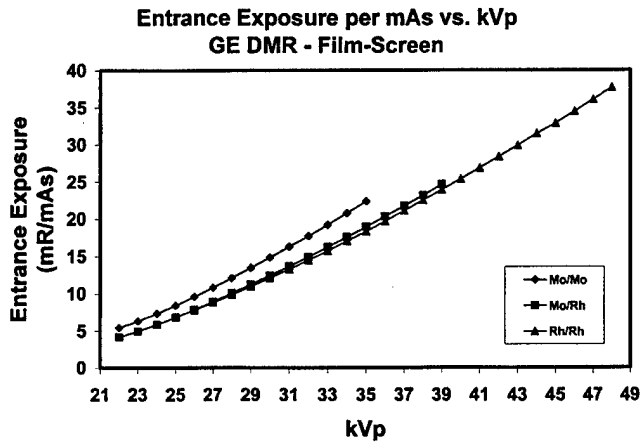

FIG. 5. Exposure output versus kVp results for the GE DMR screen-film unit.

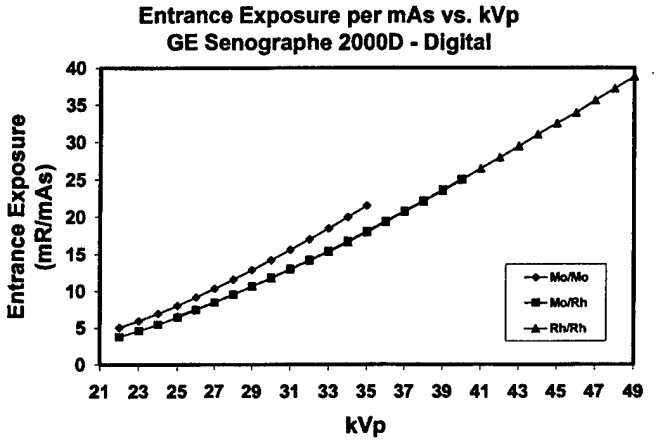

FIG. 6. Exposure output versus kVp results for the GE Senographe 2000D full-field digital mammography unit.

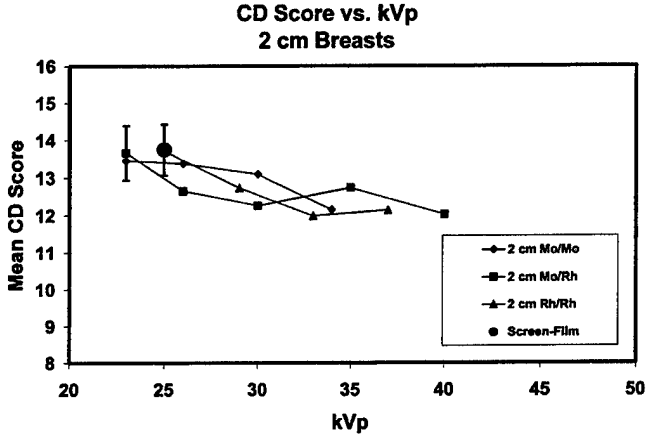

FIG. 7. CD score versus kVp for 2 cm breast thickness. The circular data point and error bars surrounding it represent the mean SFM CD score and plus and minus one standard deviation. The error bar on the highest FFDM CD score represents the mean plus and minus one standard deviation for all FFDM CD scores at this breast thickness.

Results of exposure output measurements used in the dose matching program are shown in Figs. 5 and 6 for both the GE DMR SFM unit and the GE Senographe 2000D FFDM unit. As expected, output in exposure per mAs rose as kVp increased for each target–filter combination. Output measurements were approximately consistent between the SFM unit and FFDM unit ranging from 5.0 to 22.4 mR/mAs ($1\ \text{mR} = 2.58 \times 10^{-7}\ \text{C/kg}$) for Mo/Mo, 3.8–25.0 mR/mAs for Mo/Rh, and 6.6–38.8 mR/mAs for Rh/Rh across the range of kVp values.

Results of contrast-detail imaging on the screen-film unit at 2, 4, 6, and 8 cm breast thicknesses are listed in Table I. All images had optical densities between 1.56 and 1.66, within the desired OD range for optimal detection of low-contrast lesions.[12]

Results of contrast-detail score measurements on screen-film and digital units with different target–filter and kVp combinations can be seen in Figs. 7–10. Figure 7 shows contrast-detail results of imaging a 2 cm thick breast. For the digital mammography system, the highest CD score occurred at the lowest possible kVp setting for each target–filter combination. The optimum digital mammography CD score for each of the three target–filters (13.45–13.71) was virtually identical to the optimized screen-film CD score (13.75) for 2 cm thick breasts. The significance of trends in CD score values versus kVp is discussed at the end of this section.

TABLE I. Optimal screen-film techniques with HVL, average glandular dose, and optical density results.

	Optimized screen-film techniques and data			
	2 cm	4 cm	6 cm	8 cm
Target/filter	Mo/Mo	Mo/Mo	Mo/Rh	Rh/Rh
kVp	25	25	27	28
mAs	16	85	168	283
HVL (mm Al)	0.349	0.349	0.421	0.432
Average glandular dose (mGy)	0.39	1.26	2.35	3.85
Optical density	1.56	1.66	1.58	1.59

Figure 8 shows CD results for 4 cm thick breasts using both SFM and FFDM. Most FFDM CD scores exceeded the screen-film CD score for 4 cm thick breasts. Figure 9 shows that for 6 cm thick breasts, all FFDM CD scores exceeded the optimized screen-film CD score. Figure 10 shows that for 8 cm thick breasts, FFDM CD scores using Mo–Rh and Rh–Rh target–filters were superior to those for SFM. For 6 and 8 cm thick breasts, the highest CD scores for digital occurred with Rh–Rh, regardless of the kVp selected.

Optimal digital CD scores are compared to those for SFM in Table II. For 2 cm thick breasts, there was no statistical distinction between SFM and optimum FFDM CD scores. For 4 cm breasts, optimal FFDM CD scores occurred at 24 kVp for Mo–Mo (14.20), 35 kVp for Mo–Rh (14.38), and 29 kVp for Rh–Rh (14.36). The optimal FFDM CD score for each target–filter was superior to the SFM CD score ($p = 0.013$). For 6 cm breasts, optimum FFDM CD score oc-

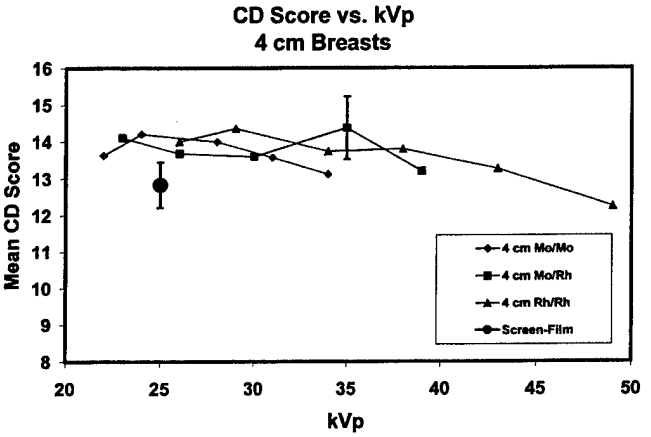

FIG. 8. CD score versus kVp for 4 cm breast thickness. The circular data point and error bars surrounding it represent the mean SFM CD score and plus and minus one standard deviation. The error bar on the highest FFDM CD score represents the mean plus and minus one standard deviation for all FFDM CD scores at this breast thickness.

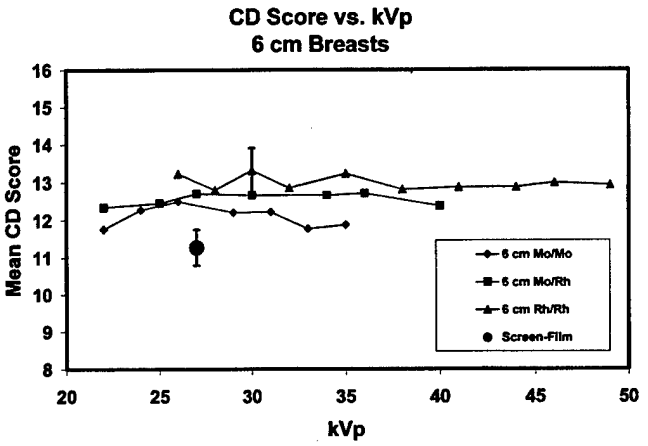

FIG. 9. CD score versus kVp for 6 cm breast thickness. The circular data point and error bars surrounding it represent the mean SFM CD score and plus and minus one standard deviation. The error bar on the highest FFDM CD score represents the mean plus and minus one standard deviation for all FFDM CD scores at this breast thickness.

curred for Rh–Rh at 30 kVp and was significantly higher than the SFM CD score (13.3 vs. 11.3, $p<0.0001$). In fact, for 6 cm thick breasts, all FFDM CD scores were higher than the SFM CD score (Fig. 9). For 8 cm breasts, optimum FFDM CD scores occurred for Rh–Rh at 46 kVp and were significantly higher than SFM CD scores (12.9 vs. 9.48, $p<0.0001$). In general, CD scores for Rh–Rh were higher than those for Mo–Mo or Mo–Rh at this breast thickness.

Trends in CD scores versus kVp at each breast thickness and target–filter combination are shown in Table III. Table III indicates that for 2 cm breasts, CD scores tended to drop as kVp increased for each target–filter material, but the trend was not statistically significant. For 4 cm breasts, CD scores also tended to drop as kVp increased; the trend was statistically significant, however, only for the Rh–Rh target–filter combination ($p=0.012$). For 6 cm thick breasts, no statistically significant trend in CD scores occurred for any target–filter combination. For 8 cm thick breasts, FFDM CD scores increased significantly as kVp increased for Mo–Mo and Rh–Rh target–filter combinations ($p<0.05$).

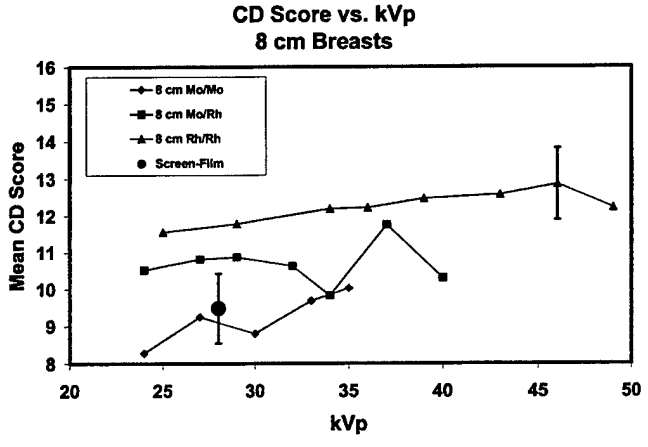

FIG. 10. CD score versus kVp for 8 cm breast thickness. The circular data point and error bars surrounding it represent the mean SFM CD score and plus and minus one standard deviation. The error bar on the highest FFDM CD score represents the mean plus and minus one standard deviation for all FFDM CD scores at this breast thickness.

TABLE II. Mean CD score comparison between screen-film and optimized digital techniques.

Mean CD score comparison underoptimized techniques			
Breast thickness	Screen-film Mean CD score	Optimal digital Mean CD score	P value
2 cm	13.8	13.5	0.47
4 cm	12.8	14.4	0.013
6 cm	11.3	13.3	<0.0001
8 cm	9.5	12.9	<0.0001

IV. DISCUSSION

Low-contrast detection in screen-film mammography was shown to be optimized by selecting Mo–Mo target–filter combinations for thin to intermediate breasts (under 5 cm) and by selecting Rh–Rh for thick breasts (over 7 cm).[10–12] With those target–filters, low-contrast detection was shown to be maximized by picking the lowest kVp that kept exposure times adequately short (under 2 s) for a given breast thickness.[12,16]

It might be expected that the optimization of technique factors in digital mammography would follow similar rules. The use of cesium-iodide as the scintillation material in digital mammography, however, instead of the gadolinium oxysulfide scintillator used in screen-film cassettes, complicates the issue. The two materials have different x-ray attenuation properties and different energy dependences of attenuation properties. In screen-film mammography, screens are required to be relatively thin to minimize blur. This, in turn, requires lower beam quality to achieve increased x-ray absorption. The linear structure of CsI crystals used as the scintillator in digital mammography reduces blur, so the CsI scintillator layer can be thicker, reducing the need for lower

TABLE III. Statistical significance of trends in CD scores versus kVp at each breast thickness and target–filter combination. The r-square value refers to the Pearson correlation coefficient obtained when a linear fit was performed on CD score versus kVp. The p value refers to the significance of the trend in CD score versus kVp.

Trend results for contrast-detail scores versus kVp				
Breast thickness	Target/filter	Mean value	R square	Trend p value
	Mo/Mo	13.0	0.855	0.075
2 cm	Mo/Rh	12.7	0.576	0.137
	Rh/Rh	12.6	0.813	0.099
	Mo/Mo	13.7	0.440	0.222
4 cm	Mo/Rh	13.8	0.119	0.569
	Rh/Rh	13.6	0.824	0.012
	Mo/Mo	12.1	0.068	0.571
6 cm	Mo/Rh	12.6	0.045	0.650
	Rh/Rh	13.0	0.147	0.274
	Mo/Mo	9.21	0.793	0.043
8 cm	Mo/Rh	10.7	0.001	0.945
	Rh/Rh	12.2	0.677	0.012

beam quality as a means to get increased absorption. The higher beam quality used in digital also increases x-ray output, thereby reducing exposure time for a given breast thickness.

The best way to determine that technique factors are optimized for the detection of low-contrast lesions in digital mammography is to conduct experiments that replicate the clinical situation as closely as possible, using the digital detector of interest. That has been done in this study using phantoms made from tissue-equivalent materials that included simulated low-contrast lesions.

Our results indicate that for a CsI scintillator and amorphous silicon detector, low-contrast lesion detection is maximized by using a softer x-ray beam (relatively low kVp) for thin breasts. Contrast-detail results for digital and screen-film mammography in thin breasts indicate that FFDM should not be expected to yield low-contrast lesion detection superior to that of SFM.

Our results indicate that for 4 cm thick breasts, low-contrast lesion detection was insensitive to the target–filter and kVp selected between 25 and 35 kVp. For thick breasts (>5 cm thick), on the other hand, low-contrast detection is maximized with this detector by selecting a harder x-ray beam. Our results indicated that at 6 cm, Rh–Rh at 30–35 kVp was optimum; at 8 cm, Rh–Rh at 40–46 kVp was optimum. This is due to the combined effect of decreased breast absorption (and therefore decreased breast dose) for higher-energy x rays in thicker breasts and higher SNR per unit dose for higher-energy x rays. The use of a harder x-ray beam for thicker breasts has the added clinical benefit of increasing x-ray output, keeping exposure times short. This has been confirmed in a separate comparison of FFDM to SFM.[16]

Our results can be compared to others that used different techniques to determine optimal beam spectra for digital mammography.[11] For the CsI-silicon diode array detector, Williams *et al.* calculated a FOM that was approximately constant as a function of kVp for all phantom thicknesses and target–filter combinations. Moreover, their FOM showed no distinction among the 3 different target–filter combinations for 3 cm thick breasts. Our results at 2 and 4 cm show no distinction among target–filter combinations, but our 2 cm results suggest a trend toward better low-contrast detection at lower kVp values.

For 7 cm thick breasts, the FOM used by Williams *et al.* indicated a preference for a Rh–Rh target–filter, but no kVp preference. In agreement with their results, our CD results for 8 cm breasts indicate that Rh–Rh is preferable to the other two target–filter combinations. In contrast to their results, our CD results indicate that higher kVp (up to 45 kVp) is preferable for thick breasts.

The SNR calculations of Williams *et al.* suggested that the Mo–Mo target–filter combination and low kVp was preferable for 3 cm thick breasts. Our CD results for 2 cm breasts concur with their results. Their SNR results found no distinction among the three target–filter combinations for thicker (7 cm thick) breasts, while our CD results find a clear preference for the Rh–Rh target–filter combination and higher kVp values for thicker breasts.

Using Monte Carlo techniques to study contrast as a function of dose for different target–filter and kVp combinations, Dance *et al.* determined that only for the thinnest breasts (2 cm thick) does Mo–Mo provide the optimal spectrum for digital mammography. For thicker breasts, Dance *et al.* determined that other target–filter combinations (Mo–Rh, Rh–Rh, Rh–Al, and tungsten–Rh) are preferable in terms of maintaining adequate SNR at a lower dose. Our results, obtained under the condition of constant breast dose for a given thickness, indicate that Mo–Rh and Rh–Rh, with even higher kVp values than those considered by Dance *et al.*, offer better low-contrast detection for breasts thicker than 5 cm.

While in this paper we focus on low-contrast detection, mammography has the additional task of detecting microcalcifications. Would the conclusions of this paper differ if the phantom had consisted entirely of graded microcalcifications? The work of Dance *et al.* suggests that for the task of maintaining an adequate SNR between calcification and background, alternative target–filter combinations producing harder x-ray beams (Mo–Rh, Rh–Rh, Rh–Al, and tungsten–Rh) would still be preferable to Mo–Mo for breasts thicker than 2 cm, although lower tube potentials (28–30 kVp) might yield the best calcification detection. The greater difference in absorption between calcifications and soft tissues at lower kVp, compared to that between fat and glandular tissues, supports this result.

The contrast-detail phantom used in this study has low-contrast targets over a uniform background. This does not fully simulate low-contrast detection in breasts, in that the phantom lacks the additional structured noise caused by fibroglandular tissues. Thus, in the experiments we have performed, the dominant source of noise limiting low-contrast detection was quantum mottle. The difficulty in simulating structured noise in contrast-detail experiments is that, unlike quantum mottle, structured noise is spatially variant. Thus, the results of CD experiments would vary depending on the specific alignment of the CD phantom with the structured noise pattern. To avoid this complication, we have included only quantum mottle noise effects. We believe that our results have clinical relevance, even in the presence of structured noise, as long as quantum mottle is not insignificant in comparison to structured noise.[17]

V. CONCLUSIONS

These results indicate that low-contrast lesion detection is optimized for a CsI silicon diode array detector under the constraint of fixed breast dose by using a softer x-ray beam for thin breasts and a harder x-ray beam for thick breasts. Under this constraint, FFDM CD scores were superior to SFM CD scores for all but the thinnest breasts.

ACKNOWLEDGMENTS

This work was supported by the Lynn Sage Breast Cancer Research Foundation and by the U.S. Army Medical Research and Material Command Award No. DAMD 17-99-1-9144.

[a]Address all correspondence to Eric A. Berns, Ph.D., The Lynn Sage Comprehensive Breast Center, Northwestern University Medical School, Galter Pavilion, 13th Floor, 251 E. Huron. St., Chicago, Illinois 60611. Telephone: 312-695-3439; fax: 312-926-6224; electronic-mail: eberns@radiology.northwestern.edu

[1]S. W. Fletcher, W. Black, R. Harris, B. K. Rimer, and X. Shapiro, "Report of the international workshop of screening for breast cancer," J. Natl. Cancer Inst. **85**, 1644–1656 (1993).

[2]J. M. Elwood, B. Cox, and A. K. Richardson, "The effectiveness of breast cancer screening by mammography in younger women," Online J. Curr. Clin. Trials **1**, 32–227 (1993).

[3]R. E. Bird, T. W. Wallace, and B. C. Yankaskas, "Analysis of cancers missed at screening mammography," Radiology **184**, 613–617 (1992).

[4]L. Ma, E. Fishell, B. Wright, W. Hanna, S. Allan, and N. F. Boyd, "Case-control study of factors associated with failure to detect breast cancer by mammography," J. Natl. Cancer Inst. **84**, 781–785 (1992).

[5]M. T. Mandelson *et al.*, "Breast density as a predictor of mammographic detection: comparison of interval and screen-detected cancers," J. Natl. Cancer Inst. **92**, 1081–1087 (2000).

[6]R. M. Nishsikawa, G. E. Mawdsley, A. Fenster, and M. J. Yaffe, "Scanned-projection digital mammography," Med. Phys. **14**, 717–727 (1987).

[7]R. Fahrig and M. J. Yaffe, "Optimization of spectral shape in digital mammography: dependence on anode material, breast thickness, and lesion type," Med. Phys. **21**, 1473–1481 (1994).

[8]L. E. Court and R. Speller, "A multiparameter optimization of digital mammography," Phys. Med. Biol. **40**, 1841–1861 (1995).

[9]D. R. Dance *et al.*, "Influence of anode/filter material and tube potential on contrast, signal-to-noise ratio and average absorbed dose in mammography: a Monte Carlo study," Br. J. Radiol. **73**, 1056–1067 (2000).

[10]W. Huda, A. Krol, Z. Jing, and J. M. Boone, "Signal to noise ratio and radiation dose as function of photon energy in mammography," SPIE Med. Imaging **3336**, 355–363 (1998).

[11]M. B. Williams *et al.*, "Beam optimization for digital mammography," *IWDM 5th International Workshop on Digital Mammography* (Medical Physics, 2001), pp. 108–119.

[12]R. E. Hendrick and E. A. Berns, "Optimizing techniques in screen-film mammography," in *Radiologic Clinics of North America: Breast Imaging*, edited by Stephen A. Feig (WB Saunders Co., Philadelphia, 2000), No. 4, pp. 701–718.

[13]X. Wu, E. L. Gingold, G. T. Barnes, and D. M. Tucker, "Normalized average glandular dose in molybdenum target–rhodium filter and rhodium target–rhodium filter mammography," Radiology **193**, 83–89 (1994).

[14]W. T. Sobol and X. Wu, "Parameterization of mammography normalized average glandular dose tables," Med. Phys. **24**, 547–554 (1997).

[15]R. G. Miller, Jr., *Beyond ANOVA, Basics of Applied Statistics* (Wiley, New York, 1986).

[16]R. E. Hendrick and E. A. Berns, "Optimizing mammographic technique," in *1999 Syllabus: Categorical Course in Diagnostic Radiological Physics; Physical Aspects of Breast Imaging—Current and Future Considerations*, edited by A. G. Haus and M. J. Yaffe (Oak Brook, IL, RSNA Publications, pp. 79–89, 1999.

[17]E. A. Berns, R. E. Hendrick, and G. A. Cutter, "Performance comparison of full-field digital mammography to screen-film mammography in clinical practice," Med. Phys. **29**, 830–834 (2002).

Appendix H

Performance comparison of full-field digital mammography to screen–film mammography in clinical practice

Eric A. Berns and R. Edward Hendrick[a)]
The Lynn Sage Comprehensive Breast Center, Northwestern University Medical School, Chicago, Illinois 60611

Gary. R. Cutter
AMC Cancer Research Center, Denver, Colorado

(Received 1 August 2001; accepted for publication 4 March 2002; published 16 April 2002)

Results of acceptance testing 18 full-field digital mammography systems for clinical use and of conducting annual physics surveys of 38 screen–film mammography systems were compared in terms of exposure times, mean glandular breast doses, and image quality. These evaluations were made using the same test tools on all systems, with emphasis on assessing automatic exposure control performance and image quality on both digital and screen–film systems using clinical techniques. Survey results indicated that digital mammography systems performed similarly to screen–film systems in terms of exposure times and mean glandular doses for thin to intermediate breasts, but that digital mammography systems selected shorter exposure times and lower mean glandular doses for thicker breasts. For all breast thicknesses, digital mammography systems yielded mean contrast–detail scores higher than those for screen–film systems. For all breast thicknesses, the 18 digital mammography systems demonstrated less variance in terms of exposure times, mean glandular doses, and contrast–detail scores than did the 38 screen–film systems tested. These results indicate that the clinical use of digital mammography may generally improve image quality for equal or lower breast doses, while providing tighter control on exposures and image quality than screen–film mammography. © *2002 American Association of Physicists in Medicine.*
[DOI: 10.1118/1.1472497]

I. INTRODUCTION

The first full-field digital mammography system was approved for clinical use by the U.S. Food and Drug Administration on January 28, 2000. During the first year of introduction, approximately 50 full-field digital mammography systems (Senographe 2000D, GE Medical Systems, Wakesha, WI) were installed for clinical use in the U.S. A similar number of FFDM units were installed outside the U.S., primarily in Europe.

While screen–film image receptors have a limited range of acceptable exposures to the image receptor, constrained by the requirement of getting adequate optical densities on the processed film, digital mammography has no similar constraint on exposure or breast dose. In fact, digital detectors are typically linear over 4–5 decades of exposure to the detector. This opens up the possibility of breast doses from digital mammography that are much higher or much lower than those from screen–film mammography. It also opens up the possibility that image quality on digital may differ from that in screen–film mammography, either due to inherent detector sensitivity differences or due to user selection of different doses to the breast.[1,2]

During the course of the last year, we have served as MQSA-qualified medical physicists in acceptance testing 18 full-field digital mammography units. During the past 2 years, we have been involved in conducting annual performance evaluations of 38 screen–film units through the Colorado Mammography Advocacy Project (CMAP).[3] During these evaluations of digital and screen–film units, measurements were made to assess the performance of these clinical systems under automatic exposure control conditions using clinical techniques. In addition to the ACR phantom, breast-equivalent phantoms of 2, 4, 6, and 8 cm thickness were used to measure exposure times, mean glandular doses, and image quality as assessed by the same contrast–detail pattern for each unit at each breast thickness.[4]

This paper compares acceptance testing of 18 of the first digital mammography systems introduced into clinical practice to annual review of 38 screen–film mammography systems.

II. MATERIALS AND METHODS

Uniform breast-equivalent (50% fibroglandular–50% fatty) materials of 2, 4, 6, and 8 cm compressed breast thicknesses were imaged using each site's clinical techniques. A single D-shaped contrast–detail (CD) phantom of our own design, now available commercially from CIRS (Computerized Image Reference Systems, Inc., Norfolk, VA), was imaged on all mammography systems. One section of the CD phantom contained a 9×9 contrast–detail pattern for assessment of simulated low-contrast lesions (Fig. 1).[4] Each row of the CD pattern contained nine circular objects at a fixed level of contrast with object diameters ranging from 0.25 mm to 4.0 mm. Each of the nine different rows had a different subject contrast, ranging from 0.3% to 4.0%.

The same single observer scored all CD images in a consistent manner using methods described previously.[4] Screen–film images were scored on a mammography viewbox with

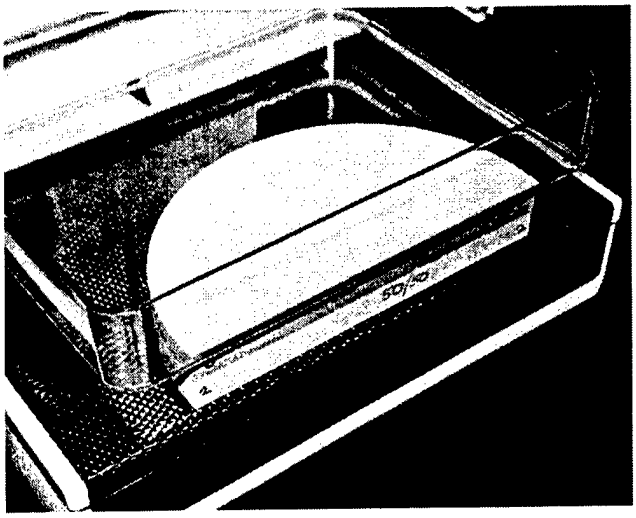

FIG. 1. Contrast–detail phantom used for both screen–film and digital mammography performance testing.

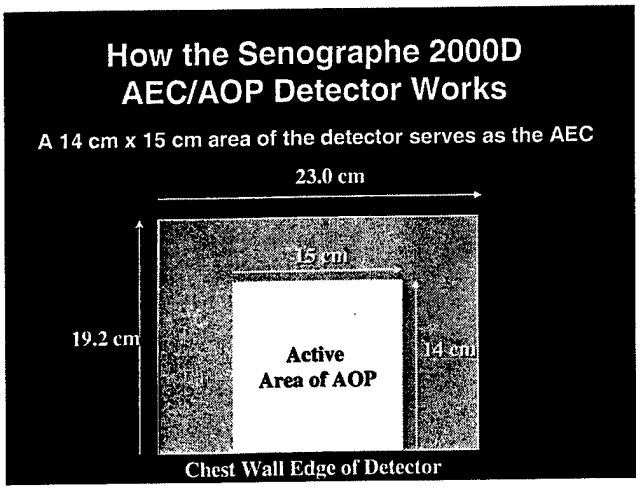

FIG. 2. Schematic of the active 14 cm×15 cm AOP area within the full-field digital detector.

complete masking and viewbox luminance exceeding 3000 cd/m^2 (nit). Digital images were scored on the system's review workstation using 2000×2500 resolution element monitors and maximum luminance of 70 footlambert (ftL) in a room with an ambient illuminance of less than 10 lumen/m^2 (lux).

In addition, the ACR mammography phantom was imaged to simulate a 4.5 cm thick compressed breast.[5]

Automatic exposure control (AEC) was used on 38 screen–film units and compared to the AEC performance of 18 GE Senographe 2000D full-field digital mammography systems. The Senographe 2000D system employs a cesium iodide scintillator coupled to an amorphous silicon diode array.[1] The array has 1920×2304 array elements uniformly distributed over a 19.2×23.0 cm field of view, each detector element being 100 microns on a side.

The GE Senographe 2000D system can function in one of three AEC (or AOP, for automated optimization of parameters) modes: AOP contrast (CNT), AOP standard (STD), or AOP dose (DOS) mode. In each of these AOP modes, a 14×15 cm area of the detector centered left-to-right and near the chest wall of the full detector is designated as the AOP sensor on the Senographe 2000D system (Fig. 2). During a 15 millisecond pre-exposure, the system takes a preliminary measurement that is used to select the target material (molybdenum or rhodium), filtration material (molybdenum or rhodium), and peak kilovoltage (kVp) setting. During the pre-exposure, the system also selects a 1×1 cm subregion of the 14×15 cm AOP detector area that serves as the active AEC sensor during the exposure that follows. The system selects the specific 1×1 cm subregion that records the lowest signal during pre-exposure. The full exposure is terminated when the selected 1×1 cm region records an adequate signal, thereby helping to ensure adequate signal and signal-to-noise ratio to the entire image.

Pixel signal-to-noise ratios (SNR) were measured in each digital mammography AOP mode using raw images. Pixel SNR was defined as the ratio of mean signal-to-signal standard deviation measured in a 1 cm^2 region of interest placed over a uniform portion of the CD phantom. SNR measured in this manner is distinct from other methods of measuring SNR and image quality,[6] and thus is referred to as "pixel SNR."

Results for exposure times, mean glandular doses, and CD scores between modalities and among FFDM modes were analyzed for statistical significance using analysis of variance methods (SAS Institute, Seattle, WA). The general linear model (PROC GLM) was used to compare measurements made at each simulated breast thickness between modalities and among the three modes used to acquire FFDM images. Satterthwaite tests (PROC T-TEST) were used to test the equality of the variances between modalities.[7]

III. RESULTS

Results in terms of exposure times, average glandular doses, and contrast–detail scores are shown in Table I and Figs. 3–5. Figure 3 demonstrates that exposure times for digital units were within the range of those for screen–film units for 2, 4, and 4.5 cm breast thicknesses, but were shorter on average for digital mammography than for screen–film mammography for 6 and 8 cm thick compressed breasts, regardless of the AOP mode used for digital ($p<0.0001$). Comparison of digital mammography exposure times using different AOP modes indicated that AOP mode selection made a significant difference in exposure times between contrast mode and the other two modes for 2, 4, 4.5, and 6 cm breasts ($p<0.001$), but made no difference for 8 cm breasts ($p>0.9$). Only for 4.5 cm simulated breasts was there a statistical distinction in exposure times between standard and dose modes ($p<0.001$). The variance in exposure times across all digital mammography units, regardless of AOP mode, was significantly lower than the variance in exposure times across all screen–film units for 2, 4, 6, and 8 cm thick simulated breasts ($p<0.0001$).

TABLE I. Comparison of exposure times, mean glandular doses, and contrast–detail scores for screen–film and digital mammography in each AOP mode at each breast thickness.

	Screen–film mammography	Digital mammography		
	Clinical technique	AOP contrast	AOP standard	AOP dose
Exposure time (seconds)				
2 cm	0.16	0.24	0.19	0.16
4 cm	0.72	0.85	0.54	0.49
6 cm	1.61	1.09	0.79	0.74
8 cm	2.91	1.69	1.69	1.70
Average glandular dose (mGy)				
2 cm	0.43	0.57	0.53	0.52
4 cm	1.19	1.47	1.28	1.06
6 cm	2.50	1.66	1.51	1.48
8 cm	4.01	3.04	3.05	3.06
Contrast–detail score				
2 cm	13.7	15.4	15.2	15.2
4 cm	13.4	14.6	14.3	14.1
6 cm	12.3	13.0	12.9	12.8
8 cm	10.6	11.8	11.9	11.9

Figure 4 demonstrates that for 2 cm breasts, mean glandular doses with digital were significantly higher than doses for screen–film, regardless of the digital mode used ($p<0.0001$). For 4 cm breasts and the ACR phantom, digital doses in AOP contrast mode were significantly higher than screen–film doses ($p<0.004$), while in AOP standard and dose modes, digital doses were significantly lower than screen–film doses ($p<0.001$). For 6 and 8 cm breasts, digital doses were significantly lower than screen–film, regardless of AOP mode selected ($p<0.0001$). Comparison of breast doses for different digital AOP modes indicated that AOP contrast had significantly higher breast dose than the other two AOP modes for 2–6 cm thick breasts ($p<0.03$). No significant difference in dose was observed between standard and dose modes for 2–6 cm breasts and no difference was found among any mode for 8 cm thick breasts ($p>0.9$). The variance in breast doses from digital mammography for each AOP mode was significantly lower than the variance in breast doses for screen–film mammography for 2, 4, 6, and 8 cm thick simulated breasts ($p<0.0001$).

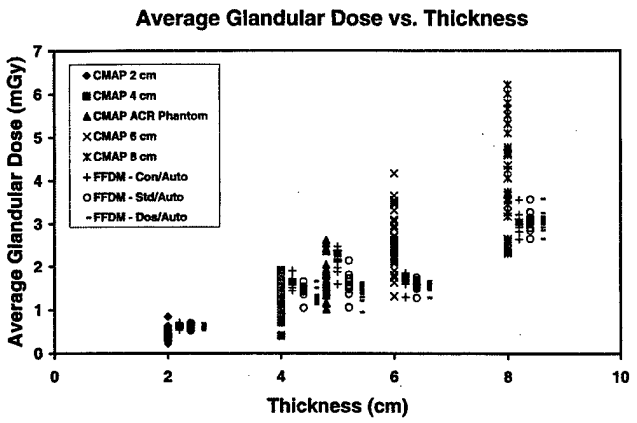

FIG. 4. Average glandular dose versus compressed breast thickness for 38 screen–film units and 18 digital mammography units in each AOP exposure mode.

Figure 5 demonstrates contrast–detail scores for both screen–film and digital mammography for 2, 4, 6, and 8 cm breast thicknesses. Results of contrast–detail experiments indicate that for each breast thickness, digital mammography provided better low-contrast lesion detection than screen–film mammography, independent of the AOP mode selected ($p<0.0001$ for 2, 4, and 8 cm, and $p<0.012$ for 6 cm thick breasts). Comparison of digital mammography contrast–detail scores indicated that selection of AOP mode had no significant effect on low-contrast lesion detection for any breast thickness. The variance in contrast–detail scores for digital from each AOP mode was lower than the variance of contrast–detail scores from screen–film mammography ($p<0.08$ for all comparisons, $p<0.05$ for 9 of 12 comparisons).

Figure 6 shows pixel SNR from digital mammography for 2, 4, 6, and 8 cm breast thicknesses. Pixel SNR fell, on average, as breast thickness increased ($p<0.001$). For each

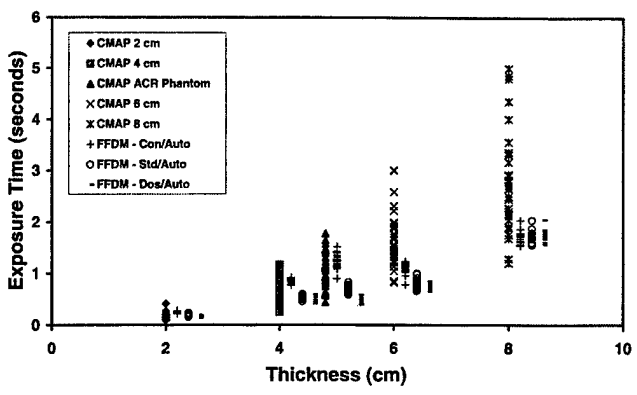

FIG. 3. Exposure time versus compressed breast thickness for 38 screen–film units and 18 digital mammography units in each AOP exposure mode.

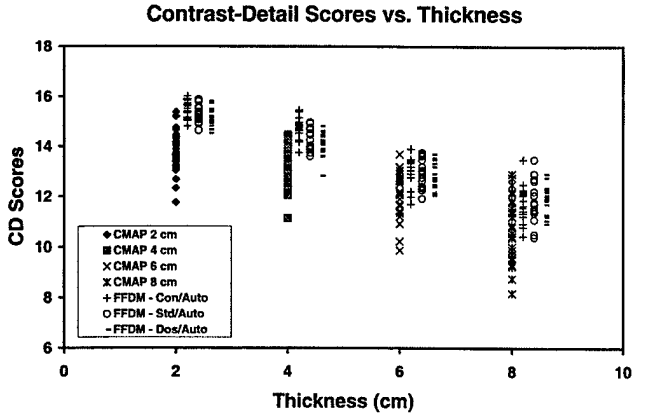

FIG. 5. Contrast–detail scores versus compressed breast thickness for 38 screen–film units and 18 digital mammography units in each AOP exposure mode.

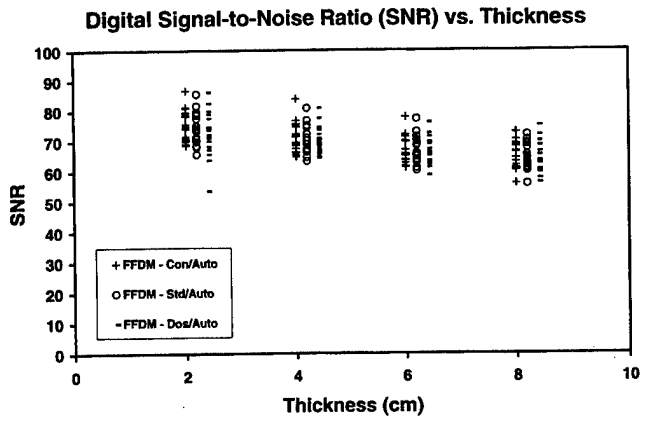

FIG. 6. Signal-to-noise ratios measured at 2, 4, 6, and 8 cm thick compressed breast thicknesses in each AOP mode for 18 digital mammography units.

breast thickness, pixel SNR values had no significant dependence on the digital AOP mode selected ($p>0.2$). For 2 cm AOP–DOS mode, one digital unit had a distinctly lower pixel SNR that the rest (Fig. 6). That low pixel SNR value was the result of the unit selecting a higher kVp than other units for a 2 cm thick breast (28 kVp), resulting in an extremely short exposure time (0.14 s). This led to the presence of residual grid lines in the image, which increased the standard deviation of the signal and decreased the pixel SNR in the resultant image.

Finally, Table II shows typical technique factors and mean exposure results for the 38 screen–film units and the 18 digital mammography units (in AOP standard mode) included in the testing.

IV. DISCUSSION

Results comparing exposure times and mean glandular doses for digital and screen–film mammography allay some possible concerns about the performance of digital mammography. For thicker breasts, where longer exposure times and higher breast doses are a potential concern, digital mammography performed better than screen–film mammography. Even for 8 cm breasts, where 82% of screen–film units yielded exposure times over 2 seconds (mean exposure time: 2.9 s), digital mammography consistently produced exposure times under 2 seconds (mean exposure time: 1.7 s). This reduction in exposure time is important in reducing motion artifacts on mammograms.

For 8 cm thick breasts, mean glandular doses averaged 3.05 mGy for AOP–STD mode digital and 4.11 mGy for screen–film; 81% of screen–film units had doses higher than 3.05 mGy. At the same time, contrast–detail scores were higher for digital (mean CD score: 11.9) than for screen–film (mean CD score: 10.6) for 8 cm thick breasts.

Table II illustrates the main reason for shorter exposure times and lower breast doses for thicker breasts on digital mammography. The table indicates that the digital AOP–STD mode picked a more penetrating beam quality for each breast thickness, with the difference increasing as breast thickness increased. For example, for 6 cm breasts, the mean half-value layer (HVL) selected by digital systems was 0.48 mm of aluminum, compared to a mean HVL of 0.38 mm of aluminum for screen–film systems. The price that might be paid for a harder X-ray beam is lower subject contract and image contrast. The effect of lower image contrast in digital mammography is offset, however, by the ability to adjust display window width to enhance contrast in the displayed digital image. As the results for thicker breasts indicate, the use of a harder X-ray beam reduces exposure time and breast dose without compromising low-contrast lesion detection.

Our results indicate that digital mammography had significantly reduced variances in exposure times and mean glandular doses, along with reduced variance in contrast–detail scores, compared to screen–film mammography at each breast thickness. Factors in the greater variability of screen–film image receptor sensitivities are the variability of system speed caused by the use of different screen–film combinations, different resultant film optical densities (ODs), and different film processing conditions. For example,

TABLE II. Comparison of typical technique factors selected by screen–film and digital mammography systems, along with resulting mean exposure, dose, and image quality measurements.

	Screen–film mammography					Digital mammography (AOP–Standard mode)				
	2 cm	4 cm	ACR Phantom	6 cm	8 cm	2 cm	4 cm	ACR Phantom	6 cm	8 cm
Target/filter	Mo/Mo	Mo/Mo	Mo/Mo	Mo/Mo	Mo/Mo	Mo/Mo	Mo/Mo	Mo/Rh	Rh/Rh	Rh/Rh
kVp	25	25	25	28	30	26	28	28	31	32
mAs	16	72	102	156	278	19	55	68	59	127
Exposure time (seconds)	0.16	0.72	1.05	1.61	2.91	0.19	0.54	0.70	0.79	1.69
HVL (mm Al)	0.33	0.33	0.34	0.38	0.41	0.35	0.37	0.44	0.48	0.49
Average glandular dose (mGy)	0.43	1.19	1.68	2.50	4.01	0.53	1.28	1.50	1.51	3.05
Optical density	1.53	1.63	1.56	1.64	1.55					
Contrast–detail scores	13.7	13.4		12.3	10.6	15.2	14.3		12.9	11.9
SNR						74	71		67	64

among the 38 screen–film units, film ODs for the ACR phantom ranged from 1.14 to 1.90 and for 6 cm breast equivalent material from 0.61 to 2.37. The high degree of variability among mammography film processing systems has been well documented.[8,9] Digital detectors eliminate target OD variability and processing variability, substituting the potential variability of detector sensitivity in its place.

The measured variability of digital detector AEC performance was considerably lower than for screen–film image receptors. Two mitigating factors are that all digital mammography data presented here were for initial acceptance of new digital systems, and, unlike the screen–film units surveyed, all digital units were from a single manufacturer. Subsequent surveys of digital mammography equipment will be needed to see if the trend of reduced variability in exposure time, mean glandular dose, and contrast–detail scores will continue as the installed base of digital mammography systems ages and as other manufacturers enter the digital mammography marketplace.

V. CONCLUSIONS

Digital mammography systems had similar exposure times and breast doses to screen–film mammography for thin to intermediate breasts, but resulted in shorter exposure times and lower mean glandular doses, on average, for thicker breasts. For all breast thicknesses, digital mammography had better detection of low-contrast simulated lesions, on average, than screen–film mammography. Digital mammography also demonstrated less variance than screen–film mammography in exposure times, mean glandular doses, and contrast–detail scores. These results indicate that clinical use of digital mammography may improve image quality for equal or lower breast doses, while providing tighter control over exposures and image quality than screen–film mammography.

[a]Author to whom correspondence should be addressed. Electronic mail: ehendrick@radiology.nwu.edu

[1]S. Vedantham, A. Karellas, S. Suryanarayanan, D. Albagli, S. Han, E. Tkaczyk, C. E. Landberg, B. Opsahl-Ong, P. R. Granfors, I. Levis, C. J. D'Orsi, and R. E. Hendrick, "Full-breast digital mammography with an amorphous silicon-based flat panel detector: physical characteristics of a clinical prototype," Med. Phys. **27**, 558–567 (2000).

[2]J. M. Lewin *et al.*, "Comparison of full-field digital mammography with screen–film mammography for cancer detection: results of 4945 paired examinations," Radiology **218**, 873–880 (2001).

[3]R. E. Hendrick, C. A. Chrvala, C. A. Plott, P. Wilcox-Buchalla, N. Jessop, and G. A. Cutter, "Improvement in mammography quality control, 1987–1995," Radiology **207**, 663–668 (1998).

[4]R. E. Hendrick and E. A. Berns, "Optimizing techniques in screen–film mammography," in *Radiologic Clinics of North America: Breast Imaging*, edited by S. A. Feig (W. B. Saunders, Philadelphia, PA, 2000), Vol. 38, Number 4, pp. 701–718.

[5]R. E. Hendrick *et al.*, Mammography quality control manual, American College of Radiology, Revised edition, 1999.

[6]D. P. Chakraborty, "The effect of the antiscatter grid on full-field digital mammography phantom images," J. Digit. Imaging **12**, 12–22 (1999).

[7]R. G. Miller, Jr., *Beyond ANOVA, Basics of Applied Statistics* (Wiley, New York, 1986).

[8]A. G. Haus and S. M. Jaskulski, *The Basics of Film Processing in Medical Imaging* (Medical Physics, Madison, WI, 1997).

[9]R. E. Hendrick and E. A. Berns, "Optimizing the selection of film and film processing in screen–film imaging," in *Advances in Film Processing Systems, Technology, and Quality Control in Medical Imaging*, edited by A. G. Haus (Medical Physics, Madison, WI, 2001), pp. 115–128.

Appendix I

Optimizing and Selecting Technique Factors for Full-Field Digital Subtraction Mammography

Materials and Methods

A special phantom was designed and built to test the effectiveness of Digital Subtraction Mammography (DSM). The phantom, designed to simulate a breast tissue composed of half fat and half glandular tissue, was built using breast equivalent material. Two sheets of the breast equivalent material (40 cm L x 20 cm W x 1 cm H), one representing only fat tissue and the other only glandular tissue, were joined together and 13 different sized Tygon tubes were placed in between. The Tygon tubing, representing blood vessels with inner diameters ranging from 0.05 mm to 3.18 mm, was set into grooves milled into both sheets of phantom material. The two plates were clamped together securing the tubing in place (Figure 1). Additional 2 cm thick pieces of breast equivalent material were added on top of the phantom to vary the thickness of the breast tissue. The contrast agent, Omnipaque 350 mgI/mL non-ionic iodine by Nycomed, was injected into the tubing using syringes and hypodermic needles of various gauges. Using reverse osmosis water, the concentration of the contrast agent was varied from 0 mg/mL to 16 mg/mL. In practice, liquid could not be injected by syringe into the smallest 3 vessels, so experiments were conducted using the largest 10 tubes, with tube inner diameter ranging from 200 microns to 3.2 mm.

Before acquiring images, a correct method of image subtraction and display had to be developed. Acquired images were sent from the GE Senograph 2000D acquisition station to a separate processing PC via a 10Mbps isolated LAN system within the department. The images were sent using DICOM protocol and received from the modality through Efilm (Canadian-developed display and transfer software for DICOM images, www.efilm.ca). Received images were processed with ImageJ (a java based shareware program offered by the NIH), where the pre-contrast image was subtracted from the post-contrast image. Subtracted images were saved as 16-bit TIFF images and opened in Adobe PhotoShop to be converted to 12-bit DICOM images using the DicomAccess plugin (DesAcc, Chicago, IL.). Either the raw data or thickness-equalized data from the modality could be processed using this method while preserving the full dynamic range. After processing, images were sent back to the modality using Efilm so the subtracted images could be viewed in the same environment with the originals.

Technique factors for image acquisition were designed under the constraint of fixed average glandular breast dose. Pre-contrast and post-contrast images for each breast thickness and contrast agent concentration used the same technique. For each thickness (2, 4, 6, 8 cm), the kVp and target-filter combination were adjusted to maintain a constant dose, decreasing the beam current (mAs) as beam quality was increased (adjusting the target-filter combination to produce a harder beam at higher kVp). A dosimetry algorithm was developed to determine the proper kVp and mAs for each thickness and target-filter combination. The algorithm was tailored to compensate for the intrinsic properties of the modality being used.

The resultant images for each breast thickness, contrast agent concentration, and exposure condition were analyzed by comparing the differences in contrast-to-noise

ratios (CNR) and the smallest visible vessel size. CNRs, reported as mean ± s.d. were determined using region of interests (ROI) placed on the same location of the largest tube and on the background signal just below this tube. Three separate readers determined vessel visibility. Contrast-detail scores were determined for each exposure condition to determine the conditions that maximize vessel detection for each breast thickness under the condition of fixed breast radiation dose at a level comparable to that of a conventional screen-film exam.

Results

The designed image subtraction methods preserved the integrity of the original images. An example of digital subtraction using a 6 cm breast phantom with 16 mg/mL contrast medium injection is shown in Figure 2. Both the pre-contrast and post-contrast images were acquired using the same techniques under a fixed average radiation dose, the target-filter combination was Mo-Mo and the exposure was at 25 kVp. The pre-contrast image (Figure 2a) was subtracted from the post-contrast image (Figure 2b). Visible in both of these images are the Tygon tubes, which also contain water, on a uniform background. In the resultant image (Figure 2c), only the differences between the two images are shown, in this case, the presence of contrast medium. Note that the walls of the Tygon tubing have been eliminated in the subtracted image.

For the 2cm breast phantom, different technique factors did not substantially change the CNR or the Contrast Detail Score. Different techniques, change in target-filter combination and change in kVp, showed no trend in increasing detection. For all concentrations, 1 mg/mL to 16 mg/mL, no technique was superior to another (Figure 3). However, increasing the concentration of contrast medium increased both the CNR and Contrast-Detail score, and smaller vessels became more visible (Figure 3).

For the 4cm breast phantom, different techniques made little difference in visibility at low concentrations of contrast medium, but showed a definite trend in higher concentrations. Using 2 mg/mL of contrast medium produced little change in the CNR between different techniques (Figure 4 a). The Contrast-detail score was fairly constant for all techniques at this concentration (Figure 4 b). As the concentration of contrast medium increased above 4 mg/mL, the CNR and Contrast-detail score improved for increasing beam quality (Figure 4 c,d). Exposures with harder beam quality, using the Rh-Rh target-filter combinations and higher energy beams, had higher CNR and Contrast-detail scores (Figure 4 c,d). The values of CNR and contrast-detail score increased in general with increasing concentration of contrast medium.

For experiments with the 6 cm and 8 cm breast phantom, exposures with higher beam quality and greater concentrations of contrast agent showed the largest improvements in CNR and Contrast-detail scores. In the 6 cm phantom, for 1 mg/mL of contrast medium, as the kVp increased, the CNR and contrast-detail score increased (Figure 5 a,b,c,d). Increasing the concentration of contrast medium, the values of the CNR and contrast-detail score increased, as shown by the figures. However, at high concentrations of contrast agent, the CNR showed an increasing trend as the beam energy increased, but the contrast-detail score did not change with increasing kVp (Figure 5c,d). At all concentrations of contrast-agent, the techniques using a harder beam (Rh-Rh target-filter combination, high kVp) had the highest CNR and contrast-detail scores. The

same trends exist for the 8 cm phantom. CNR and contrast detail scores increased with increasing concentration and increasing beam energy (Figure 6 a,b,c,d). The harder beam using Rh-Rh target-filter combinations and high kVp showed the largest increase in CNR (Figure 6 c). At high concentrations of contrast medium, the Contrast-detail score remained constant as the beam energy increased (Figure 6 d).

Discussion

Although mammography has improved the likelihood of early detection for cancerous breast lesions, many lesions still remain both clinically and mammographically occult. The false negative results of traditional screen film mammography are estimated to be around 5 to 15%. Techniques in Digital Subtraction Mammography may prove to be useful in detecting some of these lesions that otherwise would be missed. Results from this study support a trend that the use of a harder beam in contrast enhanced digital subtraction mammography will increase detection of occult lesions.

In smaller breasts, 2 to 4 cm, the choice of technique in DSM does not produce a significant difference in vessel visibility. In these cases, the choice of beam quality and contrast medium concentration do not have much impact on the CNR and Contrast-detail score (Figures 3 and 4). For thicker breasts, especially 6 cm and 8 cm breasts, these data show that a higher concentration of contrast medium increases the visibility of small vessels (Figures 5 and 6). The data show a visible trend toward using a harder beam for thicker breasts. As shown in the figures, exposures with Rh-Rh target-filter combinations result in greater CNR and better visibility of small vessels (Figures 5 and 6). Increasing the beam energy, kVp, also increases the visibility and CNR, particularly in thicker breasts. In general, a harder beam and higher energy beams should be the DSM techniques used in human studies regardless of the breast thickness. These techniques show the best results for thick breast and there is no difference in techniques for smaller breasts. Higher concentrations of contrast medium, on the order of 16 mg/mL, should also be used when evaluating the clinical significance of DSM.

The data in this study represent results from only the physics research of the imaging technique. In order for its true impact to be determined, results from a clinical trial need to be evaluated. These preliminary results pave way for clinical trials, allowing the appropriate techniques to be evaluated prior to using patients. Clinical results of DSM need to be compared against standard mammography to determine if there is significant benefit in using DSM. Once the sensitivity and specificity of the new technique are determined in the clinical study using pathological correlation, the practicality of the modality can be evaluated. While new techniques in breast MR are emerging, DSM would be a more economical choice to detect normally mammographically occult lesions. The primary advantage to DSM, besides being less costly and time consuming than MR, is that guided biopsies are much easier to perform.

Future experiments will be directed toward dual energy imaging based on the k-edge properties of the iodine contrast agent. Results from collaborative research with the University of Colorado Health Sciences Center suggest that this method may be better than temporal subtraction. In this method, two images are acquired after contrast injection. One image has a lower effective energy below the k-edge of iodine and the

other has a higher effective energy just above the k-edge of iodine. Proper filtration of the polychromatic x-ray beam will allow separation of the energy in the two exposures. This preliminary work suggests that further phantom work is needed to optimize dual energy imaging of iodinated contrast media, as is being done in this project for temporal subtraction, and then to compare the performance of the optimized dual energy approach to temporal subtraction in a group of volunteers who are going to breast biopsy.

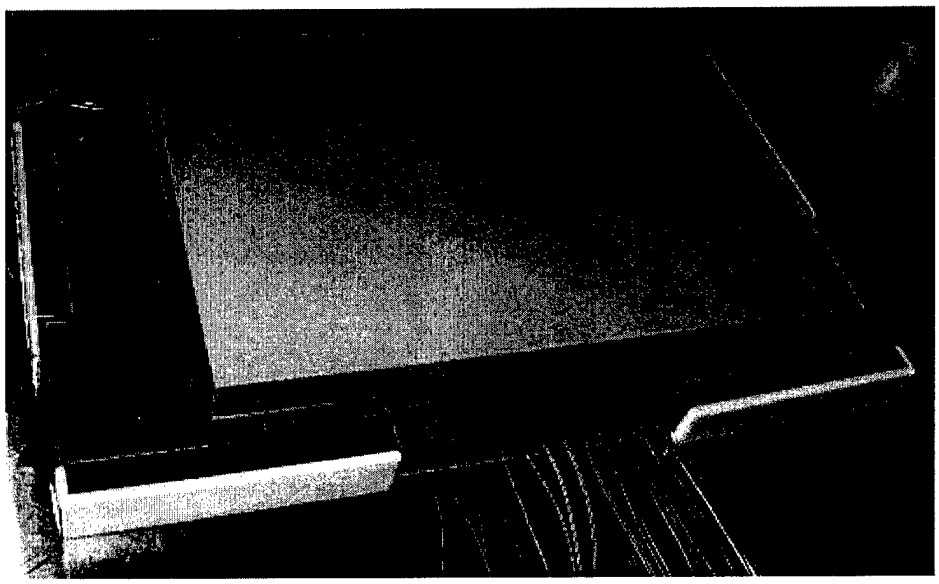

Figure 1. Experimental setup. Breast equivalent material with Tygon tubes.

Tube Inner Diameter (mm)
0.05 mm
0.10 mm
0.15 mm
0.20 mm
0.30 mm
0.56 mm
0.81 mm
1.07 mm
1.32 mm
1.52 mm
2.06 mm
2.54 mm
3.18 mm

Table 1. Tube diameters for each of the thirteen different sized Tygon tubes in the breast phantom, recorded in mm.

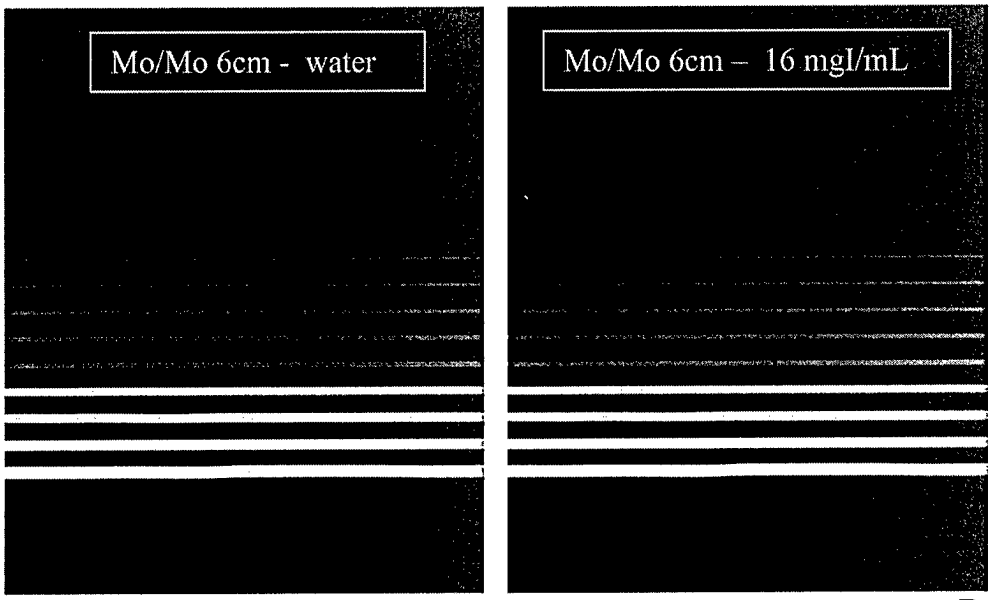

A. B.

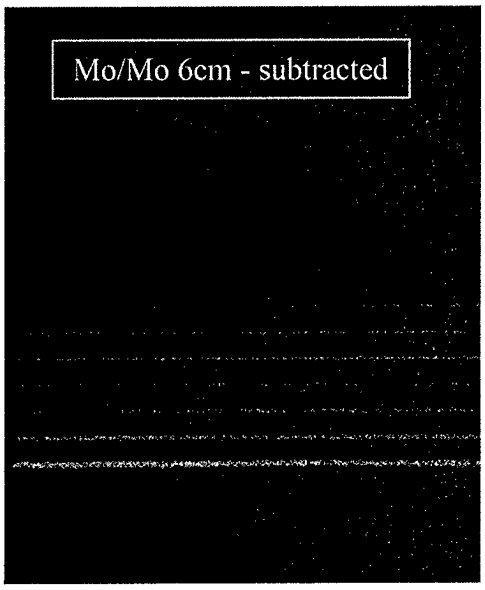

C.

Figure 2. **A.** Pre-contrast phantom image with distilled water in each tube. **B.** Post-contrast phantom image with 16 mgI/mL in each tube. **C.** Subtracted image, created by subtracting pre-contrast (A) from post-contrast (B) pixel by pixel, resulting in the difference image (C). Note that the tubes themselves are no longer visible. The image demonstrates the iodine contained within the eight largest tubes.

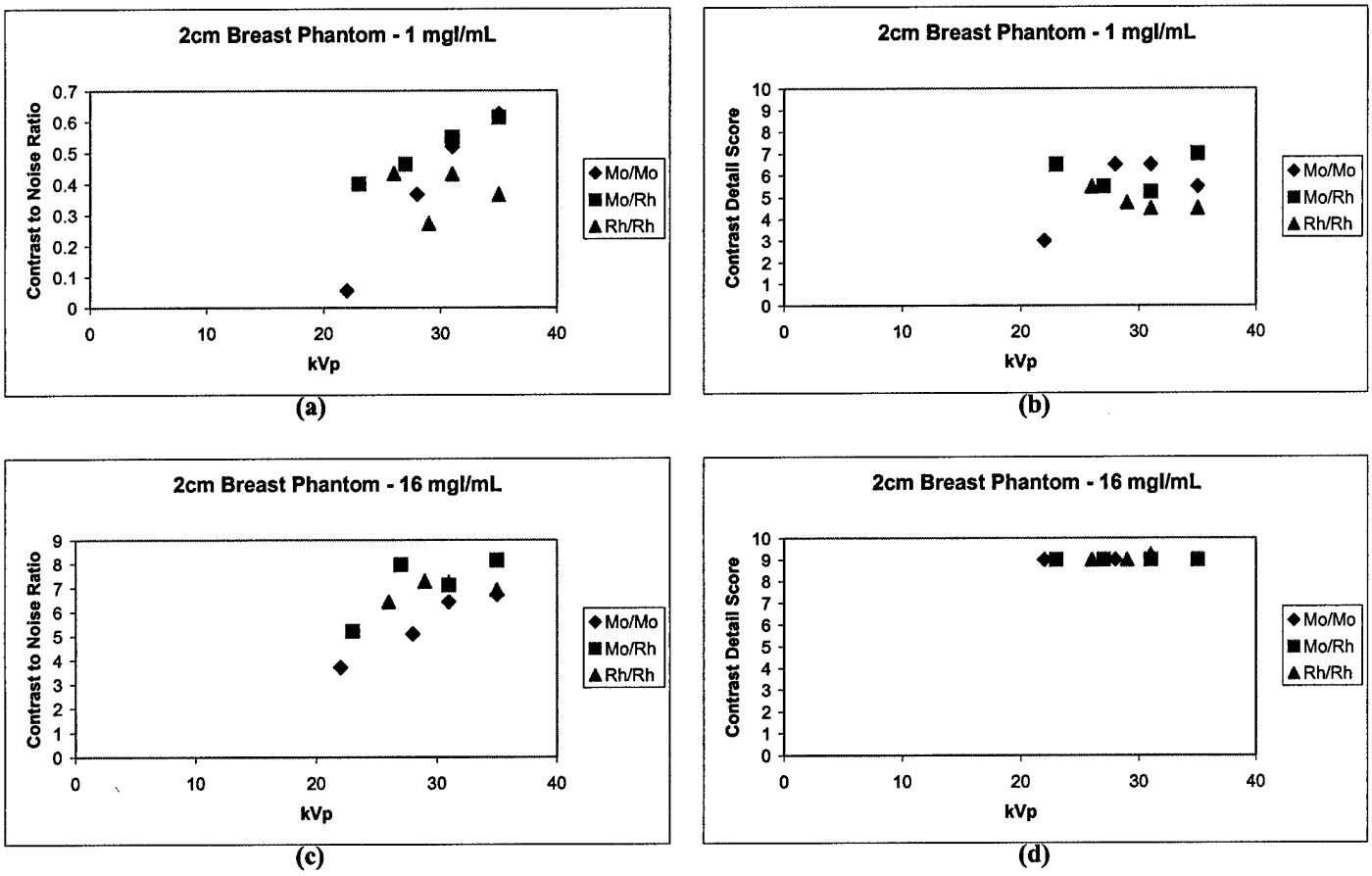

Figure 3. Results showing Contrast to Noise Ratio versus kVp for different concentrations of Iodine for three different target-filter combinations for 2 cm thick phantom.

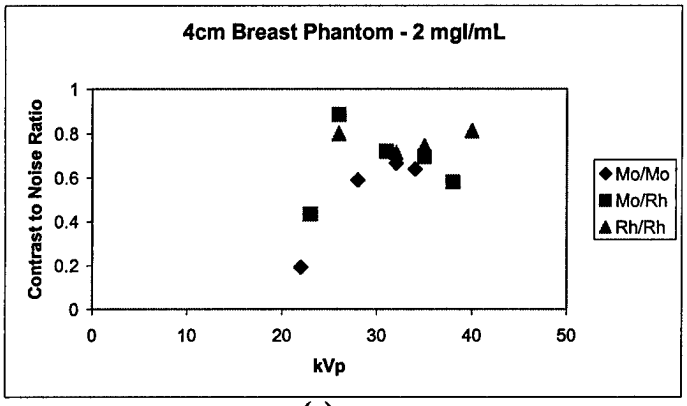

(a)

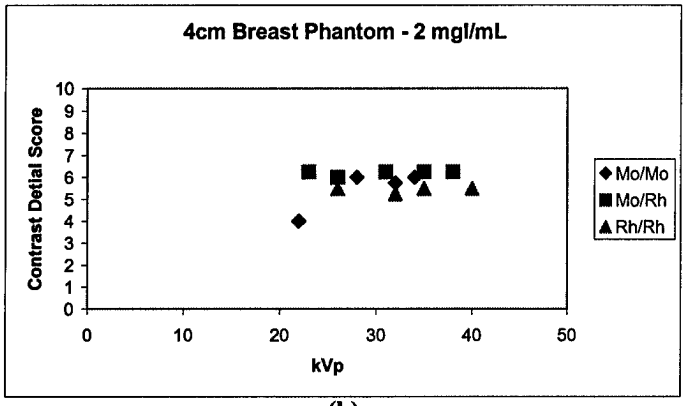

(b)

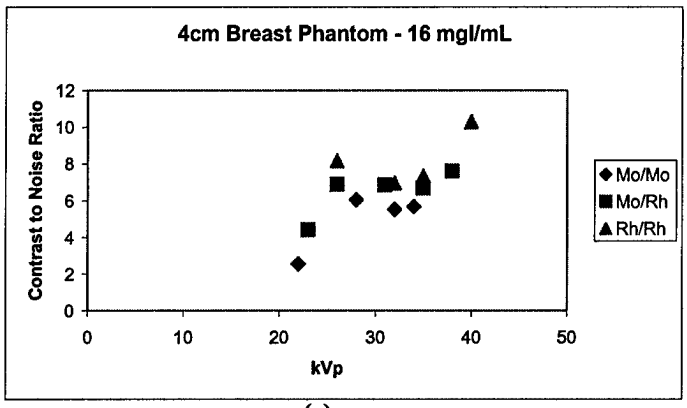

(c)

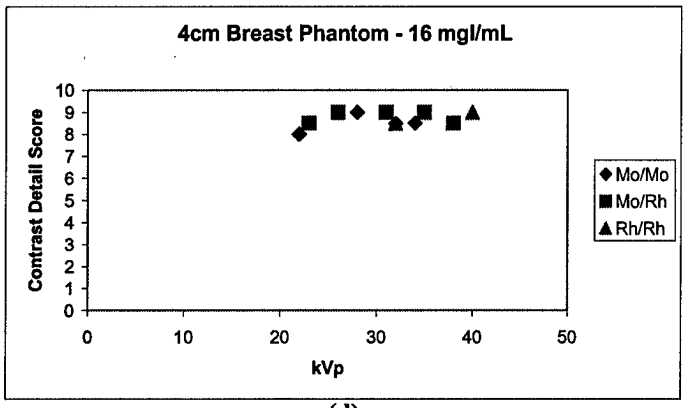

(d)

Figure 4. Results showing Contrast to Noise Ratio versus kVp for different concentrations of Iodine for three different target-filter combinations for 4 cm thick phantom.

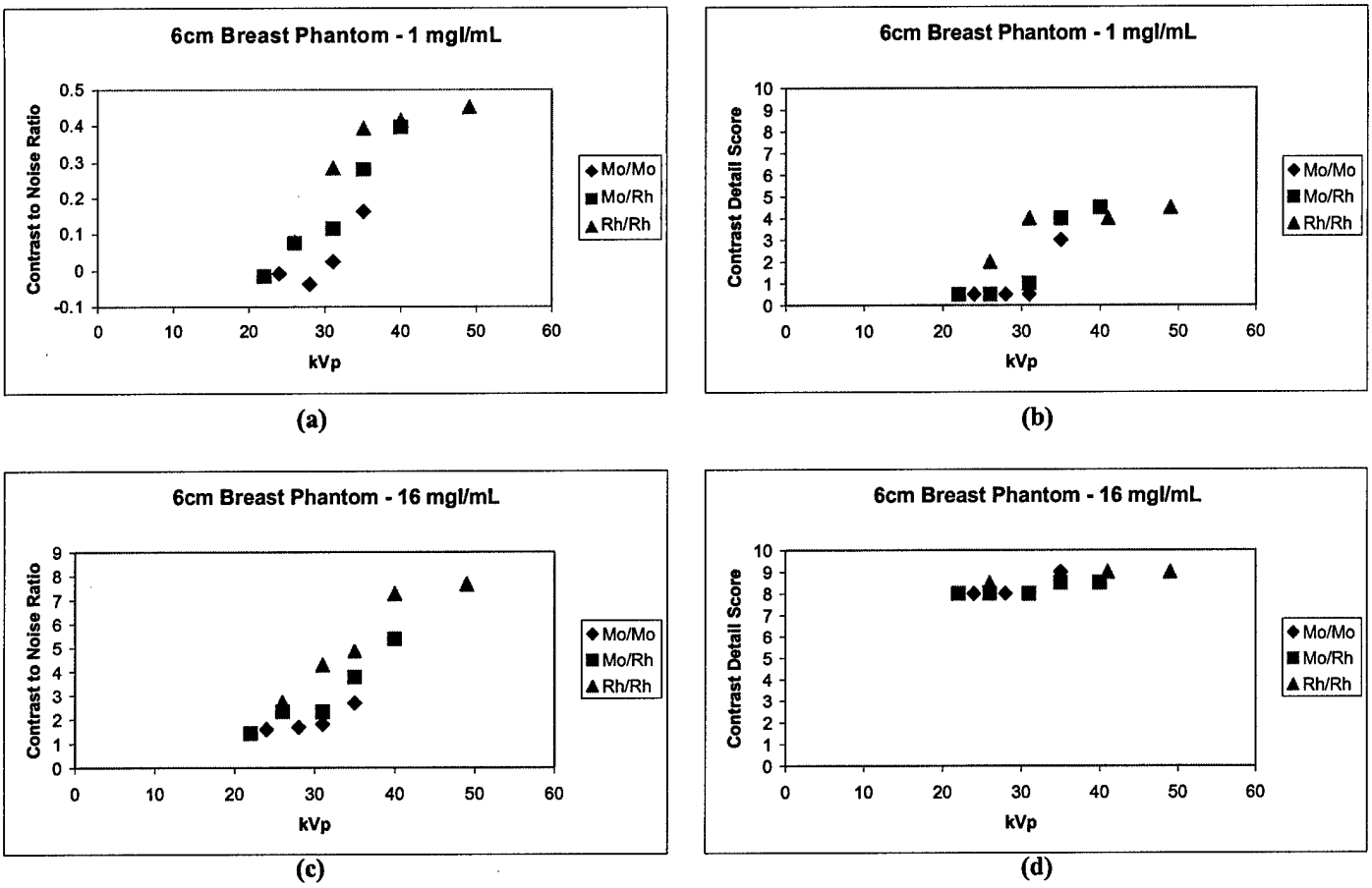

Figure 5. Results showing Contrast to Noise Ratio versus kVp for different concentrations of Iodine for three different target-filter combinations for 6 cm thick phantom.

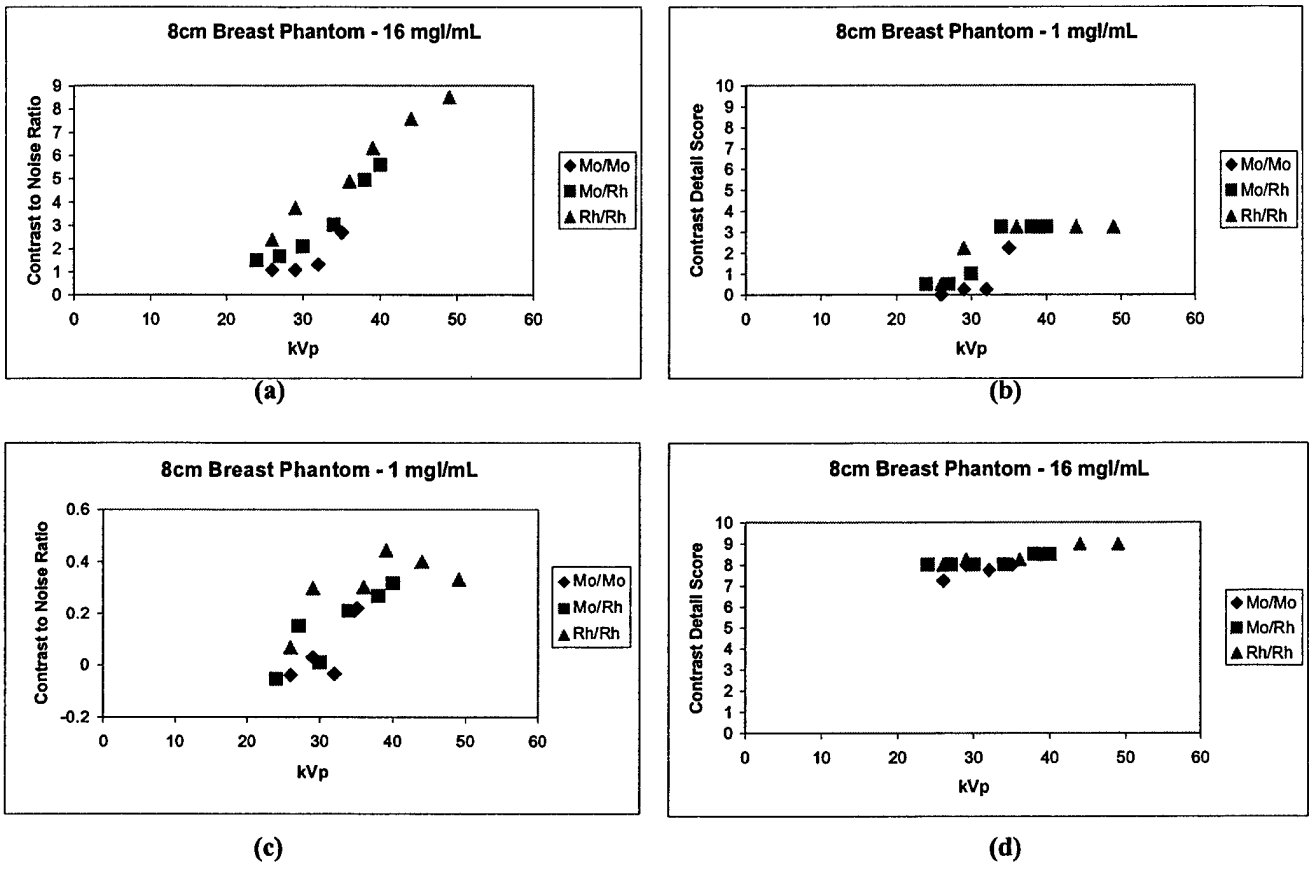

Figure 6. Results showing Contrast to Noise Ratio versus kVp for different concentrations of Iodine for three different target-filter combinations for 8 cm thick phantom.

Appendix J

AAPM 2003 Abstract

This study evaluates the effect of foam pads on mammography dose calculation. Indicated breast thickness as a function of compression force was measured for no pad, one pad, and two pads from 4 to 20 decanewtons at 2, 4, 6 and 8 centimeter (cm) breast thicknesses. Images were acquired using the mammography units AEC system using a tissue equivalent D-shaped phantom at 2, 4, 6 and 8 cm breast thicknesses. For each breast thickness, an image was acquired with no pad, with one pad (on the breast support plate), and with two pads (one on the compression paddle and one on the support plate). Technique factors were recorded and dose calculations were made using the method recommended by the ACR Mammography Quality Control Manual. For a 4.0 cm thick breast phantom compressed to 10 decanewtons with no pad, 1 pad, and 2 pads, the resulting indicated breast thicknessess were 3.5, 3.9, and 4.4 cm respectively. The no pad, 1 pad, and 2 pad dose calculations using the actual 4.0 cm thickness resulted in average glandular doses of 1.48, 1.57, and 1.59 mGy respectively, and using the indicated breast thicknesses of 3.5, 3.9, and 4.4 cm resulted in average glandular doses of 1.65, 1.60, and 1.47 mGy respectively. The results show that when using no foam pad the dose is overestimated by 11%, when using 1 pad dose is overestimated by 2%, and when using 2 pads dose is actually underestimated by 8%.

Appendix K

Era of Hope 2002 Abstract

OPTIMIZATION OF TECHNIQUE FACTORS FOR A SILICON DIODE ARRAY FULL-FIELD DIGITAL MAMMOGRAPHY SYSTEM AND COMPARISON TO SCREEN-FILM MAMMOGRAPHY WITH MATCHED MEAN GLANDULAR DOSE

Eric A. Berns, Ph.D., R. Edward Hendrick, PH.D., Gary R. Cutter, Ph.D.[2]

The Lynn Sage Comprehensive Breast Center
Northwestern University Medical School
Chicago, IL

[2]AMC Cancer Research Center
Denver, CO

Abstract

Contrast-detail image analysis was performed to optimize technique factors for detection of low-contrast lesions using a silicon diode array full-field digital mammography (FFDM) system under the conditions of matched mean glandular dose (MGD) across the full range of compressed breast thicknesses. FFDM results were compared to screen-film mammography (SFM) at each breast thickness.

Four contrast-detail (CD) images were acquired on a SFM unit with optimal techniques at 2, 4, 6, and 8 cm breast thicknesses. The MGD for each breast thickness was calculated based on HVL and entrance exposure measurements on the SFM unit. A computer algorithm was developed to determine FFDM mAs that matched MGD between FFDM and SFM at each thickness, while varying target, filter, and kVp across the full range available for the FFDM unit. CD images were then acquired on FFDM for kVp values from 23-35 for Mo-Mo, 23-40 for Mo-Rh, and 25-49 for Rh-Rh under the constraint of matching the MGD from screen-film for each breast thickness (2, 4, 6, and 8 cm). CD images were scored independently for SFM and FFDM at each technique by 6 readers. CD scores were analyzed to assess trends as a function of target-filter and kVp and were compared to SFM at each breast thickness.

For 2 cm thick breasts, optimal FFDM CD scores occurred at the lowest possible kVp setting for each target-filter and were not significantly different from SFM CD scores. FFDM CD scores decreased as kVp increased for each target-filter under the constraint of matched MGD. For 4 cm breasts, the optimum FFDM CD score was superior to the SFM CD score and decreased as kVp increased for each target-filter combination. For 6 cm breasts, optimum FFDM CD scores were significantly higher than SFM CD scores while decreasing slightly as kVp increased for Mo-Mo, but not varying significantly as a function of kVp for either Mo-Rh or Rh-Rh. For 8 cm breasts, optimum FFDM CD scores were significantly higher than SFM CD scores. For Mo/Mo and Rh/Rh, FFDM CD scores increased significantly as kVp increased.

These results indicate that low-contrast detection was optimized for FFDM by using a softer x-ray beam for thin breasts and a harder x-ray beam for thick breasts when MGD was kept constant for a given breast thickness.

Appendix L

RSNA 2001 Abstract

Title:

Clinical Performance Comparison of Full-field Digital Mammography to Screen-film Mammography

Purpose:

To compare the performance of 18 of the first full-field digital mammography (FFDM) systems introduced into clinical practice to the performance of screen-film mammography (SFM) systems already in clinical use.

Method/Materials:

During the past year, we performed acceptance tests on 18 FFDM systems. During the same period, we conducted annual performance evaluations of 38 SFM units through the Colorado Mammography Advocacy Project. Measurements were made to assess both FFDM and SFM systems under automatic exposure control using clinical techniques. In addition to the ACR phantom, breast-equivalent phantoms of 2, 4, 6, and 8 cm thickness were used to measure exposure times, mean glandular doses (MGD), and image quality as assessed by the same contrast-detail pattern for each unit at each breast thickness. FFDM measurements were taken in all 3 automated exposure modes: contrast, standard, and dose.

Results:

For standard mode, exposure times with FFDM were longer for thin to intermediate breasts ($p<0.03$), but significantly shorter for thick breasts ($p<0.0001$). For 6 cm, mean exposure time was 0.8 s (seconds) for FFDM versus 1.6 s for SFM. For 8 cm, mean exposure time was 1.7 s for FFDM versus 2.9 s for SFM. Variability of exposure times among FFDM units was significantly less than variability among SFM units.

Mean glandular doses were higher with FFDM in standard mode for thin to intermediate breasts, but lower for thick breasts ($p<0.0001$). For 6 cm, mean glandular dose (MGD) was 1.56 mGy for FFDM vs. 2.50 mGy for SFM. For 8 cm, MGD was 3.05 mGy for FFDM vs. 4.01 mGy for SFM. The variability of MGD from unit to unit for FFDM in each mode was significantly less than the variability for SFM.

Contrast-detail scores (CDS) were significantly higher with FFDM than with SFM at each breast thickness tested ($p<0.001$). For 2 cm, mean CDS was 15.2 for FFDM vs. 13.7 for SFM. For 4 cm, mean CDS was 14.3 for FFDM vs. 13.4 for SFM. For 6 cm, mean CDS was 12.9 for FFDM vs. 12.3 for SFM. For 8 cm, mean CDS was 11.9 for FFDM vs. 10.6 for SFM. The

variability of CDS from unit to unit for FFDM in each mode was significantly less than the variability for SFM.

For FFDM, mean CDS and signal-to-noise ratios (SNR) fell significantly as breast thickness increased. Both CDR and SNR values depended very little on the digital AOP mode selected.

Conclusions:

Results indicate that clinical use of FFDM should improve lesion detection, while reducing motion and breast dose for thicker breasts. FFDM provides less variability than SFM in exposure time, breast dose, and image quality.

Appendix M

RSNA 2001 Abstract

Title:

Optimization of technique factors for a silicon diode array full-field digital mammography system and comparison to screen-film mammography with matched mean glandular dose

Purpose:

To optimize technique factors for detection of low-contrast lesions using a silicon diode array full-field digital mammography (FFDM) system under the conditions of matched mean glandular dose (MGD) across the full range of compressed breast thicknesses and to compare FFDM results to screen-film mammography (SFM) results at each breast thickness.

Method/Materials:

Four contrast-detail (CD) images were acquired on a SFM unit with optimal techniques at 2, 4, 6, and 8 cm breast thicknesses. The MGD for each breast thickness was calculated based on HVL and entrance exposure measurements on the SFM unit. A computer algorithm was developed to determine FFDM mAs that matched MGD between FFDM and SFM at each thickness, while varying target, filter, and kVp across the full range available for the FFDM unit. CD images were then acquired on FFDM for kVps from 23-35 for Mo-Mo, 23-40 for Mo-Rh, and 25-49 for Rh-Rh under the constraint of matching the MGD for a given breast thickness. CD images were scored independently for by SFM and FFDM at each technique by 6 readers. CD scores were analyzed to assess trends as a function of target-filter and kVp and were compared to SFM at each breast thickness.

Results:

For 2 cm breasts, optimal FFDM CD scores occurred at the lowest possible kVp setting for each target-filter and were not significantly different from SFM CD scores (13.45 for FFDM vs. 13.75 for SFM, $p=0.47$). FFDM CD scores decreased significantly as kVp increased for each target-filter under the constraint of matched MGD.

For 4 cm breasts, optimal FFDM CD scores occurred at 23-24 kVp for both Mo-Mo and Mo-Rh. The optimum FFDM CD score was superior to the SFM CD score (14.2 vs. 12.8, $p=0.013$). FFDM CD scores decreased significantly as kVp increased for each target-filter combination.

For 6 cm breasts, optimum FFDM CD scores occurred for Rh-Rh at 30 kVp and were significantly higher than SFM CD scores (13.3 vs. 11.8, $p<0.0001$). FFDM CD scores decreased slightly as kVp increased for Mo-Mo, but did not vary significantly as a function of kVp for either Mo-Rh or Rh-Rh.

For 8 cm breasts, optimum FFDM CD scores occurred for Rh-Rh at 46 kVp and were significantly higher than SFM CD scores (12.9 vs. 9.48, $p<0.001$). For each target-filter, FFDM CD scores increased significantly as kVp increased.

Conclusions:

These results indicate that low-contrast detection was optimized for FFDM by using a softer x-ray beam for thin breasts and a harder x-ray beam for thick breasts when MGD was kept constant. Under this constraint, FFDM CD scores were superior to SFM CD scores for all but the thinnest breasts.